

Ocean feedback to tropical cyclones: climatology and processes

Swen Jullien · Patrick Marchesiello · Christophe E. Menkes ·
Jérôme Lefèvre · Nicolas C. Jourdain · Guillaume Samson ·
Matthieu Lengaigne

Received: 15 November 2013 / Accepted: 19 February 2014 / Published online: 26 March 2014
© Springer-Verlag Berlin Heidelberg 2014

Abstract This study presents the first multidecadal and coupled regional simulation of cyclonic activity in the South Pacific. The long-term integration of state-of-the-art models provides reliable statistics, missing in usual event studies, of air–sea coupling processes controlling tropical cyclone (TC) intensity. The coupling effect is analyzed through comparison of the coupled model with a companion forced experiment. Cyclogenesis patterns in the coupled model are closer to observations with reduced cyclogenesis in the Coral Sea. This provides novel evidence of air–sea coupling impacting not only intensity but also spatial cyclogenesis distribution. Storm-induced cooling and consequent negative feedback is stronger for

regions of shallow mixed layers and thin or absent barrier layers as in the Coral Sea. The statistical effect of oceanic mesoscale eddies on TC intensity (crossing over them 20 % of the time) is also evidenced. Anticyclonic eddies provide an insulating effect against storm-induced upwelling and mixing and appear to reduce sea surface temperature (SST) cooling. Cyclonic eddies on the contrary tend to promote strong cooling, particularly through storm-induced upwelling. Air–sea coupling is shown to have a significant role on the intensification process but the sensitivity of TCs to SST cooling is nonlinear and generally lower than predicted by thermodynamic theories: about 15 rather than over 30 hPa °C⁻¹ and only for strong cooling. The reason is that the cooling effect is not instantaneous but accumulated over time within the TC inner-core. These results thus contradict the classical *evaporation-wind feedback* process as being essential to intensification and rather emphasize the role of macro-scale dynamics.

S. Jullien (✉) · P. Marchesiello · J. Lefèvre · G. Samson
Laboratoire d'Etudes en Géophysique et Océanographie
Spatiales, IRD/CNRS/University of Toulouse,
14 av. Edouard Belin, 31400 Toulouse, France
e-mail: swen.jullien@gmail.com

C. E. Menkes · M. Lengaigne
Sorbonne Universités (UPMC, Univ Paris 06)-CNRS-IRD-
MNHN, LOCEAN Laboratory, IPSL, Paris, France

C. E. Menkes · J. Lefèvre
IRD, Nouméa, New Caledonia

N. C. Jourdain
Climate Change Research Centre, University of New South
Wales, Sydney, Australia

N. C. Jourdain
Laboratoire de Glaciologie et Géophysique de l'Environnement,
Université de Grenoble / Centre National de la Recherche
Scientifique, Grenoble, France

M. Lengaigne
Indo-French Cell for Water Sciences, IISc-NIO-IITM-IRD Joint
International Laboratory, NIO, Goa, India

Keywords Tropical cyclones · Air-sea coupling ·
Modeling

1 Introduction

Tropical cyclones (TCs) are strongly coupled systems. They intensify by extracting heat energy from the ocean (Emanuel 1986; Rotunno and Emanuel 1987; Holland 1997) and, in turn, provide oceanic momentum expressed as strong upwelling and asymmetric mixing that result in sea surface temperature (SST) cooling under the eye and eyewall (e.g., Price 1981; Shay et al. 1989; Jullien et al. 2012). The main objective of this study is to improve our understanding of coupling processes controlling TC intensity. The SST feedback effect, i.e., the sensitivity of TC intensity to

Table 1 Negative SST feedback effect on TC central pressure from various sources and models

References	Data type	ΔSST (°C)	ΔP (hPa)	$\Delta P/^\circ C$ (hPa °C ⁻¹)
Holland (1997)	Static theory			33
Schade (2000)	Dynamic theory			21–45
Bender et al. (1993)	Idealized static storm model	5.6	16.4	2.9
Bender et al. (1993)	Idealized moving storm (7.5 m s ⁻¹) model	2.6–3	7.3	2.6
Bender and Ginis (2000)	Model of realistic events	3	10–40	3–13
This study	20-year Realistic model	0–6	0–30	0–15

ΔSST is storm-induced SST cooling in °C and ΔP the difference of TC central pressure between forced and coupled models in hPa. The sensitivity of storm intensity to SST cooling is given in hPa °C⁻¹

TC-induced cooling is generally investigated and discussed from theoretical and case studies. Thermodynamic arguments (Holland 1997; Schade 2000) suggest a large negative SST feedback on storm intensity, reducing the cyclone's maximum potential intensity (MPI) by 21–45 hPa °C⁻¹. This sensitivity is much higher than that of storm intensity to the ambient (large-scale) SST estimated from thermodynamic theory (Emanuel 1988: 10 hPa °C⁻¹) or observations (e.g., Demaria and Kaplan 1994: 10–20 hPa °C⁻¹). However, sensitivity to SST cooling is lower in modeled case studies than theoretical predictions with values of about 10 hPa °C⁻¹ or less (Bender et al. 1993; Bender and Ginis 2000). Table 1 provides a short summary of the SST feedback effect from various studies.

Numerous factors may affect storm-induced SST cooling and feedback. Slow translation speed and shallow ocean mixed layer depth (MLD) appear to favor stronger SST cooling and negative feedback (Sutyrin and Khain 1984; Schade and Emanuel 1999). Schade and Emanuel (1999) from a simple coupled model propose a range of 10–60 % decrease of storm intensity depending on their motion speed. Other subsurface oceanic features such as thermocline stratification or fine scales associated with fronts and eddies also have potential to affect storm intensity (Schade and Emanuel 1999; Bao et al. 2000; Wu et al. 2007; Vincent et al. 2012b). The deepened mixed layer of warm-core eddies for example are known to promote TC intensification (e.g., Chang and Anthes 1978; Sutyrin and Khain 1984; Bao et al. 2000). However, these results are only based on isolated events studies and no statistical description has yet been proposed for ocean eddy effect on TC activity.

Independently from the cooling process, the feedback effect invoked by thermodynamic theories may also be overestimated. Paradigms for TC intensification based on

thermodynamic considerations generally assume that surface moisture fluxes in the core region have a direct control on the growth rate of storms by a linear instability mechanism between evaporation and tangential wind speed (the WISHE mechanism of (Emanuel 1986). Other paradigms attempt to include more explicitly the role of intra-eyewall dynamics (Schubert et al. 1999; Yang et al. 2007; Montgomery et al. 2009; Wang and Wu 2004), and that of the TC secondary circulation, i.e., radial advection driving humidity convergence (Charney and Eliassen 1964; Ooyama 1969) and absolute angular momentum (Smith et al. 2009). If radial convergence is an essential process of intensification, then the local effect of SST feedback on air–sea fluxes must be integrated in a macro-scale dynamical framework.

In addition to its effect on TC intensity, idealized model experiments suggest that ocean coupling has some impact on storm tracks and translation speed (Bender et al. 1993; Bender and Ginis 2000), the latter owing to alteration of the beta drift.

Comparative forecasts of TCs with operational uncoupled and equivalent coupled models show that coupling substantially improves the forecast of TC intensity (Bender and Ginis 2000; Sandery et al. 2010). Three-dimensional oceanic features (MLD, eddies, stratification...) are of primary relevance in these experiments and suggest that the use of simple mixed layer models is not adequate to assess the effect of coupling. However, realistic coupled model applications have been limited to either short-time storm events or coarse resolution climate studies that only produce cyclone-like vortices (Scoccimarro et al. 2011). The present study is based on a regional, mesoscale coupled model of the South Pacific region [139.6°–200.0°E, 31.4°–1.6°S] to provide a climatology of tropical cyclone–ocean interactions in the present climate. Twenty years of simulation (1979–1999) and about 160 tropical cyclones provide some statistical reliability that is generally missing in event studies. This approach has already been used with success to study the South Pacific climatology of tropical cyclones (Jourdain et al. 2011) and its oceanic response (Jullien et al. 2012) in non coupled modes (forced atmosphere or forced ocean). Here, we pursue the same approach, adding the coupling effect. First, the impact of coupling on TC distributions is assessed by comparing forced and coupled simulations. Then, the processes at play in the control of TC intensity by the ocean are investigated.

2 Models and methods

2.1 Atmospheric model

In this study, the Weather Research and Forecasting (WRF) model version 3.3.1 is used with the Advanced Research

WRF (ARW) dynamic solver (Skamarock and Klemp 2008). ARW was specially designed with high-order numerical schemes to enhance the model's effective resolution of mesoscale dynamics (Skamarock 2004). The configuration and choice of parametrization is very similar to that of Jourdain et al. (2011) and was selected to realistically represent the large-scale environment and related tropical cyclone activity in the Southwest Pacific. Physical parametrizations include the Betts–Miller–Janjic (BMJ) convective scheme; the Yonsei University (YSU) planetary boundary layer (PBL) with Monin–Obukhov surface layer parameterization; the WRF single-moment three-class microphysics scheme (WSM3); the Dudhia shortwave radiation scheme; and the RapidRadiation Transfer Model (RRTM) for long-wave radiation. The surface drag coefficient is given by the classical Charnock relation. The model simulations use 31 terrain-following vertical levels with refinement in the PBL. Horizontal refinement is provided through a two-way nesting procedure. The coarser grid with 105 km resolution encompasses the Indo-Pacific region [89.8°–240.2°E, 41.2°S–21.6°N] and the inner grid with 35 km resolution encompasses the South Pacific Convergence Zone (SPCZ) region [139.6°–200.0°E, 31.4°–1.6°S]. Boundary and surface forcing for the coarser grid are from the 6-hourly National Centers for Environmental Prediction Reanalysis 2 (NCEP-2 reanalysis; Kanamitsu et al. 2002).

A detailed sensitivity study to model parameterizations is presented in Jourdain et al. (2011). A similar investigation was repeated here (our WRF version was upgraded from that used by Jourdain et al. 2011) but rather focusing on air–sea interactions. The usual difficulty of coupled models, even at regional scales is the added freedom of SST and air–sea fluxes to drift away from the observed state, indicating a loss of the initial surface heat balance. This loss can largely be attributed to inaccurate physics parametrizations and our selection in this respect proved satisfactory in preventing important drift.

The largest coupled model sensitivity is found on the choice of shortwave radiation parametrization. Specifically, we dismissed the Goddard radiative scheme implemented in WRF that produced excessive surface heat flux resulting in warmer surface temperatures than observed (over land and ocean). In turn, the associated change in surface pressure produced overly-strong winds converging from the north to the SPCZ. Accurate wind observations provided by the QuikSCAT scatterometer proved useful as a proxy for assessing the surface heat flux consistency with dynamical balance.

Surface drag is another key feature of air–sea interactions as it represents the ocean–wave–atmosphere interface. If the Charnock relation (Charnock 1955) is generally considered valid for intermediate wind speed and mature waves, measurements in extreme wind conditions suggest an increase of

the drag coefficient due to the presence of young seas (as theorized by Janssen 1989) but at the same time some form of saturation due to various possible wind-wave decoupling mechanisms (Powell et al. 2003; Donelan 2004). In WRF, the Donelan relation which causes drag saturation at high wind speed was made available for hurricane studies but our sensitivity experiments showed that it worsens the regional wind and SST climatology (and TC climatology as well). This appears to result from a drag reduction in the Donelan compared with Charnock relation even at intermediate and low wind speeds. Drag saturation (if confirmed) is only expected for extreme winds, which are very rarely attained with our 35-km grid resolution (maximum wind speed is rarely up to 35 m s⁻¹ in the model). We thus consider our study in the range of validity of the Charnock relation.

The parameterization of convection is less directly relevant to air–sea interactions but is crucial for both an accurate representation of the SPCZ and the cyclogenesis process; it was thoroughly tested by Jourdain et al. (2011) who found the best behavior with BMJ (also the simplest and cheapest option in WRF). With similar experiments, we could confirm their result in the coupled model.¹

WSM3 is a cheap and simple scheme for microphysics. Rain and snow are combined into a single variable, as are cloud water and ice. There is no representation of mixed phase microphysical processes: freezing occurs instantaneously and completely at the first level where the temperature is colder than 0 °C, and melting occurs similarly one level below the freezing level. In a cloud resolving application of WRF, Stern and Nolan (2011) show a relatively weak sensitivity of microphysics schemes (including WSM3 and more complicated ones) on TC intensification. Microphysics in our mesoscale application is mostly involved in the maturing phase of TCs associated with strong grid-scale updrafts (precipitation is otherwise due to subgrid-scale convection). The neglect of mixed phase processes may affect the detailed process of diabatic heating at this point but with no large consequences (Stern and Nolan 2011).

Finally, we also confirmed the good agreement between model and observations using the YSU closure scheme, a K profile parameterization with non-local mixing that is

¹ In BMJ, Janjić (1994) introduced a cloud efficiency parameter to improve the original Betts–Miller scheme. This allows a modulation of the precipitation response to a change of the environment by acting on the timescale of convective adjustment (set between 1 and 2 h). A lower cloud efficiency gives longer adjustment timescale and weaker convective precipitation. Cloud efficiency has different values in various WRF releases and is higher in the 3.3 than in the 2.2 release used by Jourdain et al. (2011). We kept the default V3.3 parameters, which generally provided more realistic precipitation patterns at the price of somewhat excessive summer rainfall. This choice of parameters generally improved the spatial distribution of cyclogenesis.

better suited to convective regimes than other local closure models implemented in WRF (see also Hill and Lackmann 2009).

2.2 Ocean model

The ocean model used is the Regional Oceanic Modeling System (ROMS; Shchepetkin and McWilliams 2005). ROMS solves the primitive equations in an Earth-centered rotating environment, based on the Boussinesq approximation and hydrostatic vertical momentum balance. In this study, we use the ROMS-AGRIF version of the model that has a compact package for implementation of realistic configurations (Penven et al. 2006; Debreu et al. 2012). It is a split-explicit, free-surface ocean model, discretized in terrain-following coordinates with high-order numerical methods for reduction of numerical dispersion and diffusion errors. Associated with a 3rd-order time stepping, a 3rd-order, upstream-biased advection scheme allows the generation of steep gradients, enhancing the model's effective resolution (Marchesiello et al. 2011). Because of implicit diffusion in the advection scheme, explicit lateral viscosity is unnecessary, except in sponge layers near the open boundaries where it increases smoothly close to the lateral open boundaries. For tracers, a 3rd-order upstream-biased advection scheme is also implemented but the diffusion part is rotated along isopycnal surfaces to avoid spurious diapycnal mixing and loss of water masses (Marchesiello et al. 2009; Lemarié et al. 2012). A non-local, K-profile planetary (KPP) boundary layer scheme (Large et al. 1994) parameterizes the unresolved physical vertical subgrid-scale processes at the surface, bottom and interior of the ocean. If a lateral boundary faces the open ocean, an active, implicit, upstream biased, radiation condition connects the model solution to the surroundings (Marchesiello et al. 2001). The model was thus developed for regional applications and its computational methods allow for realistic, long-term integrations in a fine-mesh regional domain.

The oceanic configuration used in the coupled study is very similar to that described in Jullien et al. (2012) with few changes given in the following summary. The configuration was processed with ROMSTOOLS (Penven et al. 2008), a collection of global data sets and a series of Matlab programs collected in an integrated toolbox for generating the grid, initial conditions, and open boundary data. The vertical grid has 51 terrain-following levels with 2–5 m resolution in the first 50 m, 10–20 m resolution in the thermocline and 50–250 m in the deep ocean. The oceanic domain is the same as the inner atmospheric domain [139.6°–200.0°E, 31.4°–1.62°S] with the exact same grid and same 35 km horizontal resolution (no interpolation is needed to transfer data between the ocean and atmosphere). The interannual oceanic forcing is from

the ORCA025-G70S global ocean simulation at a quarter degree resolution (Barnier et al. 2006) and applied at open boundaries with the mixed active/passive conditions described above. Initialization is also from ORCA025-G70S; the simulation starts in January 1979 with a model spin-up that ends well before the cyclonic season of 1979–1980 (the first considered in our analyses).

2.3 Coupling procedure

Air–sea coupling is performed in the high-resolution SPCZ domain, i.e., on the 35 km grid shared by both oceanic and atmospheric models. The coupled simulation ran for 20 years over the present climate (1979–1999).

The oceanic and atmospheric models are coupled using a global in time Schwarz method within a simple Fortran coupler designed by Lemarié (2008). The coupling frequency is 3 h, a multiple of the baroclinic time steps of the atmospheric model (5 min) and oceanic model (30 min). The coupling algorithm consists in three steps:

1. Advancing the atmospheric solution on a 3-h time window, using the ocean model SST of the last time window (or the initial SST field at initialization)
2. Averaging surface momentum, heat and fresh water fluxes from the atmospheric model over the 3-h time window
3. Advancing the ocean model for the same 3-h time window using surface fluxes computed at step 2.

This algorithm does not strictly ensure consistency of surface fluxes in the oceanic and atmospheric models because the oceanic model forcing is a function of SST computed on the previous time window. The original iterative procedure of the Schwarz method was designed to correct this problem and thereby suppress a form of coupling instability (Lemarié 2008). This would be particularly useful for climate studies using low frequency coupling but has an extra computational cost. Here, the relatively high coupling frequency of 3 h appears to avoid the instability problem even without correction and the results are weakly sensitive to the converging procedure. At this frequency, the diurnal cycle and storm displacement are also properly resolved. On the other hand, very high coupling frequency should be avoided as bulk flux formulations are uncertain at time-scales of less than an hour (Large 2006). For this reason also, the use of time-averaged fluxes is preferable to instantaneous fluxes.

Note that the ocean model computes a bulk rather than skin SST that requires very fine surface resolution. The skin SST has a larger diurnal variability (particularly in the Pacific warm pool area) that directly impact air–sea fluxes. For more realism in the estimation of these fluxes in WRF, a sea surface skin temperature is computed from the

scheme of Zeng and Beljaars (2005). It consists of prognostic, one-dimensional heat transfer equations for the molecular sublayer (cool skin) and diurnal layer (warm skin) of the ocean. It provides the difference of temperature between the skin temperature at the top of the cool skin and the bulk temperature (given by the model SST) at the bottom of the warm layer. The ocean model bulk SST is here taken at 10 m depth for consistency with the scheme of Zeng and Beljaars (2005). Our simulations show realistic 0.5–2 °C diurnal variations of skin SST and a mean difference between bulk and skin SST of about 0.25 °C. The skin SST is colder in average due to heat loss in the cool skin by long-wave radiation. As expected, a sensitivity test using bulk rather than skin SST for the computation of surface fluxes (not shown) revealed that the use of skin SST slightly reduces the surface heat and moisture fluxes to the atmosphere. However, the regional climate and cyclonic activity did not appear greatly affected by this choice.

2.4 Forced simulation setup

A twin uncoupled atmospheric simulation (hereafter called *forced simulation*) is performed in order to analyze the impact of coupling on tropical cyclones. The forced simulation is computed using exactly the same WRF configuration and SST fields from the coupled simulation, but the latter are reprocessed to remove TC-induced cold wakes. Cold wake removal is done by a 90 day low-pass FFT filter applied at each location of TC occurrence over a 3 degree radius disk and from 1 day before occurrence (cyclones by their large size have an effect ahead of their core) to 20 days after. Then, the high-frequency ambient SST (which is filtered in the same time as the storm-induced cooling) is injected back in the cyclone track by interpolating fields from the sides of the TC track. As a result, the forced simulation has no ocean feedback from TC occurrence but keeps all other oceanic impact. An example of cold wake filtering is presented in Fig. 1.

It is important to note that even the small SST perturbations produced by the filtering method are enough to change the course of chaotic events in the present climate. Tropical cyclones in the forced simulation are independent events from the coupled cyclones. Their genesis time and trajectories are different and, therefore, rarely cross the filtered SST locations. Therefore, they are weakly affected by the choice of filtering methods. The downside is that the two simulations are only comparable at a statistical level, not for particular events.

2.5 Tracking methodology

The tracking method used in this work was developed by Chauvin et al. (2006) and used in Jourdain et al. (2011)

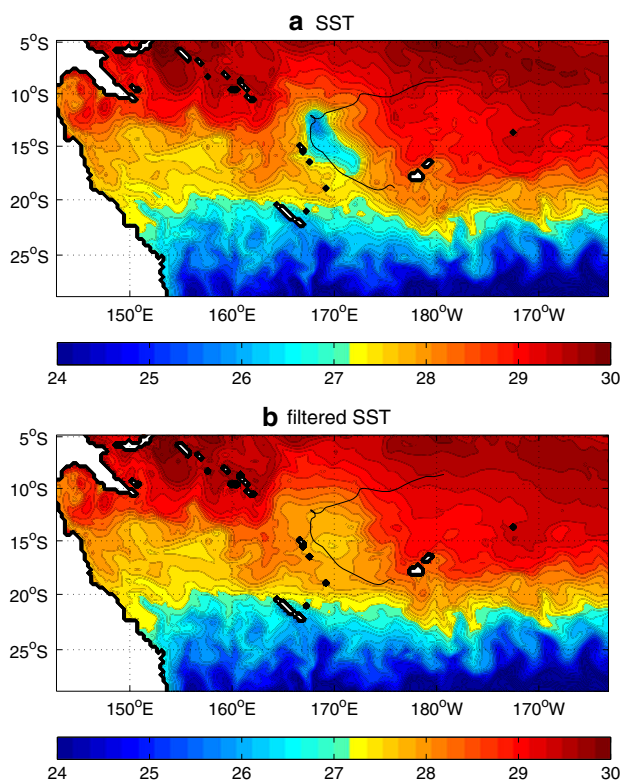


Fig. 1 Example of a TC cold wake event and its filtering procedure: **a** SST field from the coupled model (°C), **b** filtered SST field used in the forced model

with few modifications. Several criteria are used to distinguish tropical cyclones from various tropical disturbances or intense mid-latitude systems at each time step:

- Mean sea level pressure is a local minimum
- 850 hPa vorticity $>VOR$
- Maximum 850 hPa wind speed $>WT$
- Mean 700–300 hPa temperature anomaly $>TT$
- 300 hPa temperature anomaly >850 hPa temperature anomaly
- 850 hPa tangential wind >300 hPa tangential wind

where VOR, WT and TT are threshold parameters. Anomalies are defined as the difference between the system and its environment (defined using the radius of maximum radial pressure gradient; see Chauvin et al. 2006). The tracks are then constructed by an iterative process that links the points where the criteria are satisfied. As a final step, all criteria except “850 hPa vorticity $>VOR$ ” are relaxed so that the tracks are completed both backward and forward. This relaxation method prevents a cyclonic system whose intensity decreases and then increases again from being counted twice.

The WT threshold can be objectively determined following Walsh et al. (2007). An empirical choice of the two other thresholds was made by testing different values of the criteria and verifying that the detected systems were actual

tropical cyclones. The thresholds retained for this study are:

$$\text{VOR} = 20.10^{-5} \text{ s}^{-1}, \quad \text{WT} = 17 \text{ m s}^{-1} \quad \text{and} \quad \text{TT} = 1 \text{ K}.$$

Since VOR and TT thresholds are empirical, the sensitivity of the tracking method to their choice was investigated as in Jourdain et al. (2011). A positive TT criteria is important to detect warm core vortices, whereas excessive values fail to detect all tropical cyclones. The vorticity threshold has a significant role in filtering weaker meso-scale vortices.

2.6 Compositing methodology

As mentioned above, the direct comparison of particular events between forced and coupled simulations is impossible due to the chaotic nature of the simulations. However, we can construct composite cyclones in various ways in order to compare statistical quantities along cyclone tracks. The composite methodology of Jullien et al. (2012) was used again for its robustness. Three types of composites are presented here: an *Eulerian composite*, a *cross-track composite* and an *along-track Lagrangian composite*. As a first step, TC characteristics are extracted along the tracks of all simulated events.

Specifically, on each TC location where wind speed reaches at least 17 m s^{-1} , a cross track section is extracted by interpolation of all fields on a finer cross-track grid (10-km resolution). To avoid “smearing” the strong eyewall features during the compositing of all TCs, the interpolated fields are re-centered on the minimum wind location and normalized by their radius of maximum winds. After normalization, the composited TC track is rescaled by the mean radius of maximum winds. This procedure is efficient in constructing a smooth but realistic composite of tropical cyclones.

The Eulerian composite is built by looking at cross-track sections around the time of TC occurrence: from 10 days before to 30 days after passage. Eulerian composite analyses are thus presented as a function of time around occurrence, which we call ‘lag’. It represents an Eulerian view: at any given location, the storm is shown to approach, pass through and get away.

Finally, an along-track Lagrangian composite is built by averaging TC variables over a 400-km cross track distance around the track center at the TC passage time. Each TC is then normalized by its duration and the final composite is rescaled by the mean duration. It creates an along-track composite that represents a Lagrangian view of a composited TC life cycle (intensification, mature phase and decay).

3 Environmental conditions

3.1 The ocean-atmosphere interface

Climatological 1979–1999 summer SST computed from the coupled simulation (Fig. 2a, b) is presented here as an end product of surface oceanic conditions. The model SST is in good agreement with southwest Pacific observations and shows no drift over the 20-year simulation (not shown). This suggests a consistent representation of air–sea exchanges that validates our choice of physical parametrization, particularly the shortwave radiation scheme and turbulent exchange parameters. The net heat flux seasonal cycle (Fig. 3b) is similar to observations, albeit with lower values, but the accuracy of heat flux observation is much lower than that of SST as illustrated by large discrepancies among observational products. A generally better accuracy is attributed to QuikSCAT surface scatterometer wind data (Figs. 2c, d, 3a), validating the model representation of SPCZ circulation. We see the trade wind confluence in the east and convergence of trade winds and Australian monsoon winds in the west (monsoon winds are slightly overestimated). The correct representation of surface dynamics is an indirect validation of its surface thermodynamic forcing. In addition, the coupled model shows no drift or instability associated with the added degree of freedom.

In the SST map of Fig. 2a, b, we identify two important subregions: the Coral Sea [145° – 170° E, 5° – 18° S] and the warm pool region [170° – 200° E, 5° – 15° S]. The latter is a warm SST region with relatively deep oceanic mixed layer (Fig. 4a, b shows the model MLD, which favorably compares with estimations by de Boyer Montegut et al. 2004). The Coral Sea is slightly cooler and features shallower mixed layer. Section 7 will unveil a strong regional modulation of coupling strength pertaining to the dependence of SST on thermocline structure under mixing and upwelling conditions.

3.2 SPCZ and cyclogenesis index

The environmental conditions of cyclogenesis are essentially related to convective potential, wind shear, mid-tropospheric humidity, and vorticity (Gray 1975). The localization of maximum convective potential is given by the SPCZ position (Fig. 5a, b *dashed* and *solid lines*). It is computed as the meridional maximum precipitation in both observations (Tropical Rainfall Measuring Mission 3B-42 gridded product; Adler et al. 2000) and the coupled simulation. Model and observations are in very good agreement showing the same classical east-west tilt of maximum precipitation that is reminiscent of

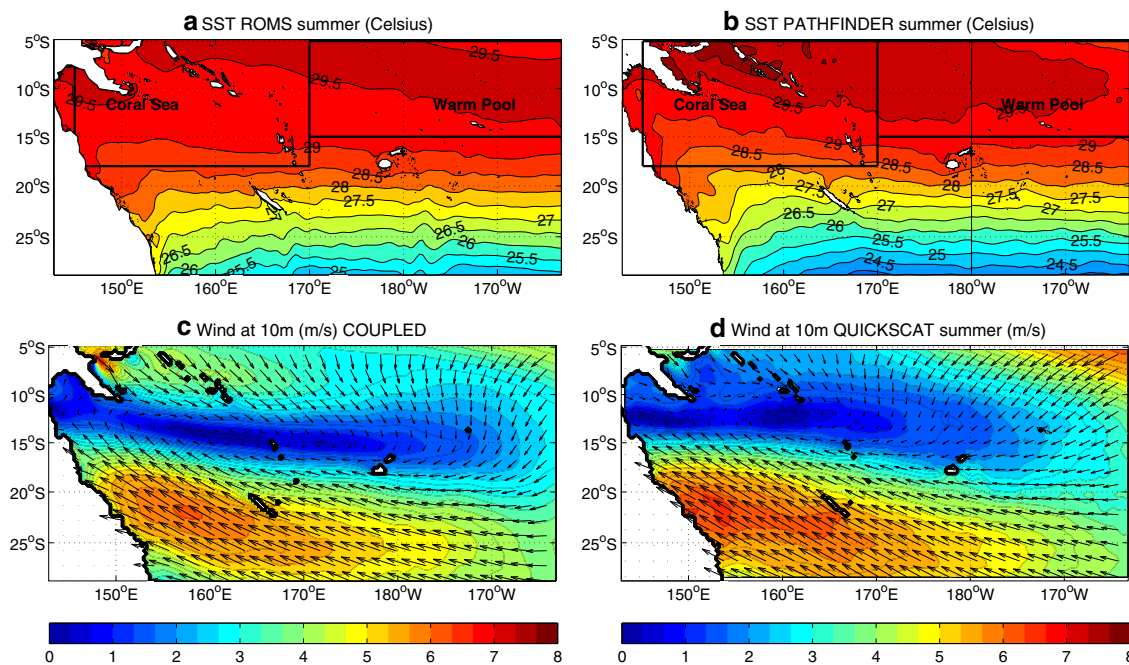


Fig. 2 Mean austral summer (January–March) **a, b** SST (°C) and **c, d** 10-m wind speed (m s^{-1} , shaded area) and vectors. The *left panels a, c* show the 1979–1999 coupled model solution and the *right panels b, d* the observed climatology; **b** Pathfinder (dataset developed by the

NASA Physical Oceanography Distributed Active Archive Center and the NOAA National Oceanographic Data Center); **d** QuikSCAT 1999–2009

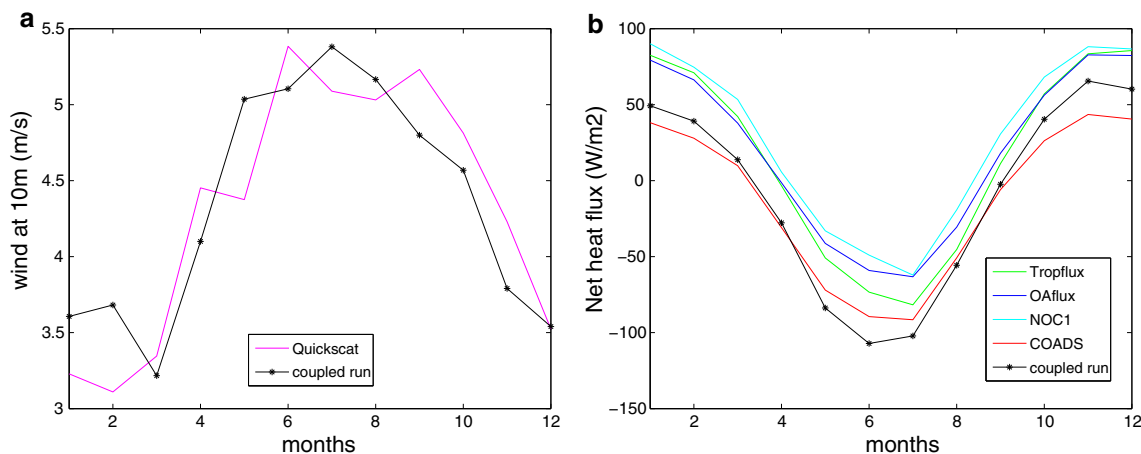


Fig. 3 Seasonal cycle of **a** 10-m wind speed (m s^{-1}) and **b** surface net heat flux (W m^{-2}) from the 1979–1999 coupled model (*black line*) and various observational datasets (*colored lines*): QuikSCAT 1999–2009 (*purple line*; <http://cersat.ifremer.fr>); TropFlux 1979–1999 (*green line*; <http://www.locean-ipsl.upmc.fr/~tropflux/>

data); OAflux 1979–1999 (*blue line*; <http://oaflux.whoi.edu>); NOC1 climatology (*cyan line*; <http://www.noc.soton.ac.uk/science-technology/earth-ocean-system/atmosphere-ocean/>); and COADS climatology [*red line*; Comprehensive Ocean-Atmosphere Data Set (COADS; Slutz et al. 1985; da Silva et al. 1994)]

surface wind convergence patterns (Fig. 2c, d). This result is not trivial as evidenced by the failure of climate models (Walsh et al. 2004; Jourdain et al. 2011; Brown et al. 2013).

Next, the combined effect of all atmospheric conditions favorable to cyclogenesis is represented by the Convective Yearly Genesis Potential Index (CYGP; Royer et al. 1998) computed as follows:

$$CYGP = \underbrace{|f| I_{\xi} I_S}_{dynamic} \underbrace{k}_{thermal} (P_C - P_0) \tag{1}$$

where f is the Coriolis parameter in 10^{-5}s^{-1} , $I_{\xi} = \xi_r \frac{f}{|f|} + 5$ with ξ_r the relative vorticity at 925 hPa in 10^{-6}s^{-1} , $I_S = (|\frac{\partial V}{\partial P}| + 3)^{-1}$ with $\frac{\partial V}{\partial P}$ the vertical shear of the horizontal wind between 925 and 200 hPa in $\text{m s}^{-1}/755 \text{ hPa}$, k is an

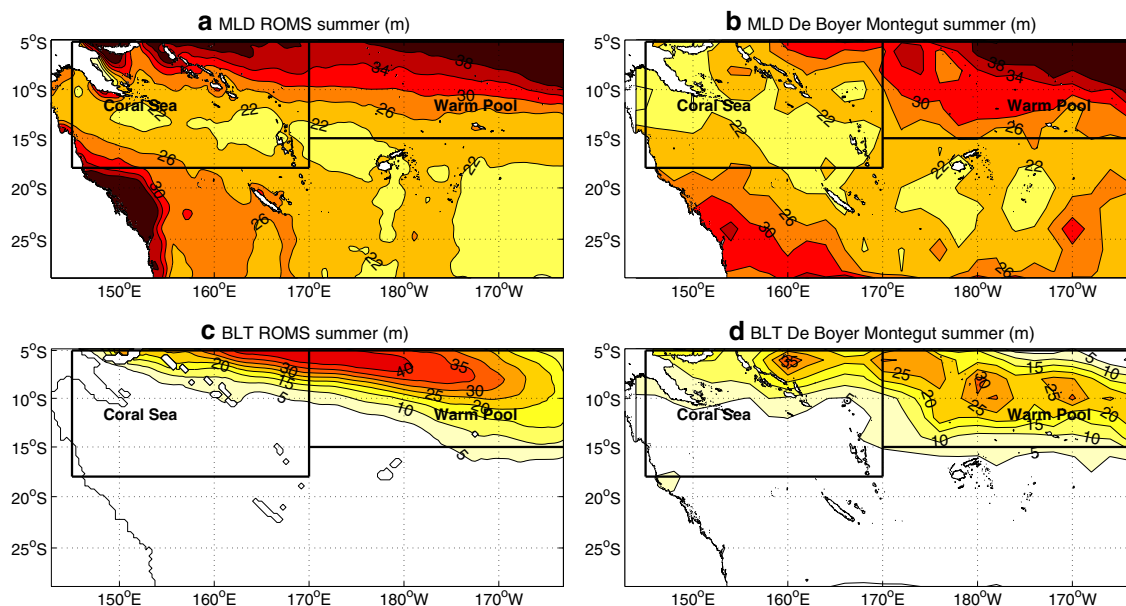


Fig. 4 Mean austral summer (January–March). **a, b** Mixed layer depth (MLD, m), **c, d** barrier layer thickness (BLT, m) from the 1979–1999 coupled model (**a, c**) and observed climatology from de Boyer Montegut et al. (2004) (**b–d**); **b** MLD with fixed criterion in

density of 0.03 kg m^{-3} difference from surface (<http://www.ifremer.fr/cerweb/deboyer/mld>); and **d** BLT computed as thickness of the layer between the MLD and the depth of the isotherm SST- $0.2 \text{ }^{\circ}\text{C}$

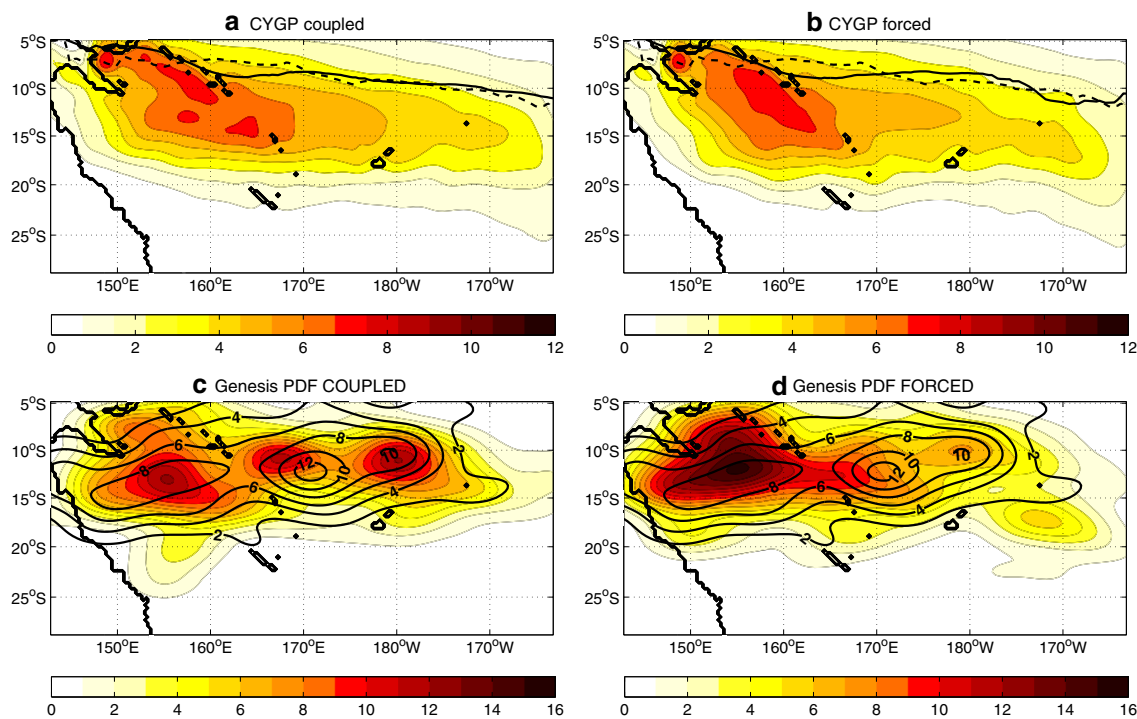


Fig. 5 a, b Mean yearly CYGP index and **c, d** PDF of cyclogenesis (in number of TCs per 5° and per 20 years, normalized to the observed number of TCs) for the coupled model (**a, c**) and the forced model (**b, d**). The *black solid and dashed line* in (**a, b**) represents

arbitrary constant adjusted to produce the right number of cyclones, P_C is the convective precipitation in mm day^{-1} and P_0 is a threshold below which the convective potential

summer SPCZ position respectively in the model and TRMM 3B-42 gridded product observations (Adler et al. 2000). Black contours overlaid on the *shaded plots* in (**c, d**) present the PDF of cyclogenesis from SPEARTC observations

is set to zero to avoid spurious cyclogenesis off the tropics. We chose to use this cyclogenesis index (with $P_0 = 3$) in agreement with Menkes et al. (2012) for its good

performances in the South Pacific. CYGP (Fig. 5a, b) shows favorable conditions of cyclogenesis slightly south of the SPCZ position, i.e. near the maximum of vorticity. The region of highest potential cyclogenesis given by CYGP is the Coral Sea [145°–170°E, 5°–18°S] as in observations (see Vincent et al. 2011).

4 TC structure

The composited TC structure of the coupled model is presented in Fig. 6 as a function of cross track distance from the cyclone eye (the right-hand side of the plot represents the left-hand side of the storm which is strongest in the southern hemisphere; we choose this convention for easier comparison with studies of the northern hemisphere) and pressure vertical levels. This analysis emphasizes the persistent properties of simulated cyclones and filters the anomalies of isolated events. It can thus be thought of as an archetypal phenomenon. In Fig. 6, we selected TCs with wind speed higher than 27 m s^{-1} to emphasize the characteristics of TC structure. The composite computed from all weak ($17\text{--}27 \text{ m s}^{-1}$) and strong ($>27 \text{ m s}^{-1}$) events is similar but with less amplitude and asymmetry.

The composited TC presents all features of observed cyclones (e.g., Gentry and Lackmann 2010; Stern and Nolan 2011; Jourdain et al. 2011, for a selection of observations for model validation). The warm core temperature (Fig. 6a) has the classical V-shape structure, with 6 K maximum anomaly (over 10 K for some individual events) located in the upper troposphere (200–400 hPa) and a ridge through the outflow layer. There is also a second midlevel maximum around 600 hPa. The warming of the core of tropical cyclones is one of its most emblematic attribute. It is supposedly due to a combination of diabatic heating in the eyewall updraft and dry adiabatic descent within the eye (a forced response to the eyewall heating in the Sawyer-Eliassen secondary circulation). However, the inner core temperature profiles, including the magnitude of upper- and mid-level maxima, are still debated (Stern and Nolan 2011).

Relative humidity anomaly in the TC core relative to ambient humidity (Fig. 6b) shows a 40–45 % increase in mid-troposphere (400–700 hPa) with larger values on the strong side. Vertical velocities (Fig. 6c) present tilted and asymmetric updrafts along the eyewall with values of up to 0.4 m s^{-1} in the composite, although they can reach more than 1.5 m s^{-1} in individual TCs.² The eye structure is well

represented by a minimum of vertical velocity and even some subsidence appearing in the composite between 400 and 600 hPa (there is smoothing in the composite as individual events show subsidence variably extending to the top but the mid-level maximum seems the most robust feature).

Radial and tangential velocities present a very strong asymmetry (Fig. 6d, e). The main radial inflow is in the surface Ekman layer, it converts into eyewall updraft (maximum above the boundary layer) and the main outflow is at 150 hPa. Surface inflow is forced by tangential winds that are maximum in the eyewall in the upper boundary layer (suggesting supergradient winds in the inner-core; Smith and Montgomery 2010) and decreases with height, consistent with gradient wind balance in a warm core system (note the anticyclonic flow aloft at larger radii). The radius of maximum winds is about 100 km, which is larger than the mean observed value of 50 km but expected from a mesoscale resolution model (Gentry and Lackmann 2010). The cyclone's secondary circulation is thus composed of a frictionally forced circulation added to the forced response to eyewall convection. The absolute angular momentum (Fig. 6f; $M = rv + \frac{1}{2}fr^2$, with r , v and f the radial distance, tangential velocity and Coriolis frequency), as described in Smith et al. (2009), emphasizes the dynamical role of radial convergence in amplifying tangential winds above the boundary layer in the outer-core. The removal of M by friction counteracts its strong radial influx in the boundary layer but the patterns of M and v towards the inner-core suggest some boundary layer spin-up there as well (strong vorticity in the inner-core effectively increases the Coriolis parameter; see Smith et al. 2009).

Figure 7 presents cross-track profiles of surface properties for weak ($17\text{--}27 \text{ m s}^{-1}$) and strong ($27\text{--}37 \text{ m s}^{-1}$) TC categories. The 10-m wind speed profile features a clear cyclone eye with strong wind drop off in the center and asymmetric eye wall. Stronger winds appear on the storm's left-hand side because of the addition of TC translation speed on the left-hand side and subtraction on the right-hand side. Note that the decay of tangential winds away from the center is relatively mild. A leftward SST cooling asymmetry (Fig. 7b) results from this TC wind pattern but also from wind-current resonance at near-inertial periods (Shay et al. 1989; Jullien et al. 2012; Vincent et al. 2012a). SST cooling by the strong composited TC is almost twice as much as that of the weak TC, i.e., $1.9 \text{ }^\circ\text{C}$ at the maximum. This value for individual events can reach $6 \text{ }^\circ\text{C}$ but maximum cooling generally lags maximum wind forcing and thus occurs in the cyclone wake, i.e., outside the inner-core region. This remark is important for feedback effects that will be analyzed later in this paper.

² The sloping of the eyewall results from the action of centrifugal forces on ascending air parcels as pressure gradient decreases. The slope is tightly related to the warm core and tangential wind structure and thereby dependent on grid resolution, steeper for coarser models (e.g., Gentry and Lackmann 2010).

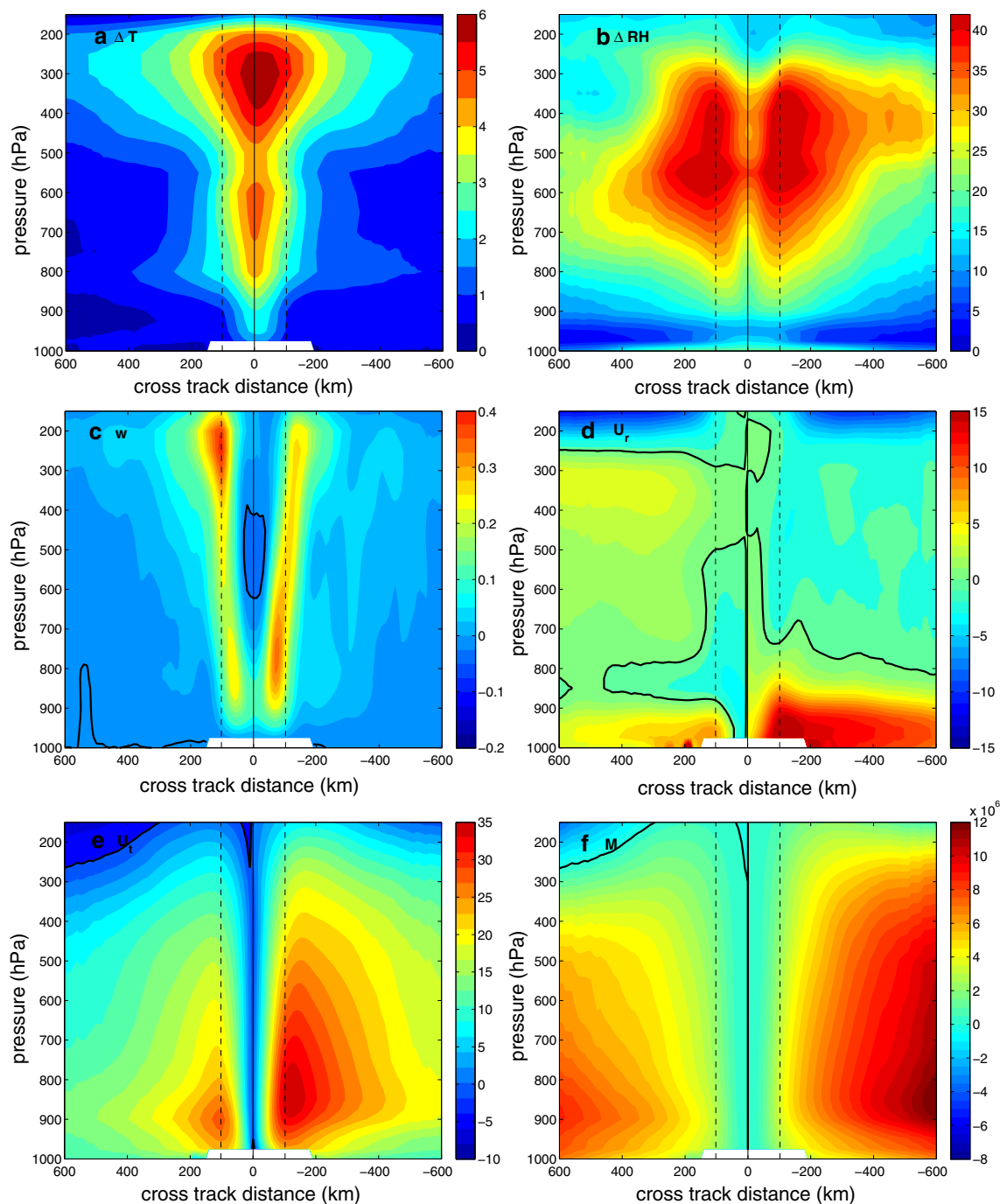


Fig. 6 Cross track sections of the coupled model composite TC, based on all events with wind speed $>27 \text{ m s}^{-1}$. **a** Warm core anomaly ($^{\circ}\text{C}$); **b** relative humidity anomaly (%); **c** vertical velocity (m s^{-1}); **d** radial velocity (m s^{-1}); **e** tangential velocity (m s^{-1}); and **f** absolute angular momentum per unit mass ($\text{m}^2 \text{ s}^{-1}$). The coordinates are the cross track distance (in km) and vertical pressure levels

(in hPa). Ambient values of temperature and humidity (needed to construct anomalies) are pre-storm time-mean values between days -10 and -2 . The vertical *dashed lines* represent the averaged radius of maximum winds; the vertical *solid line* shows the TC center; the *solid bold lines* in velocity plots represent zero values

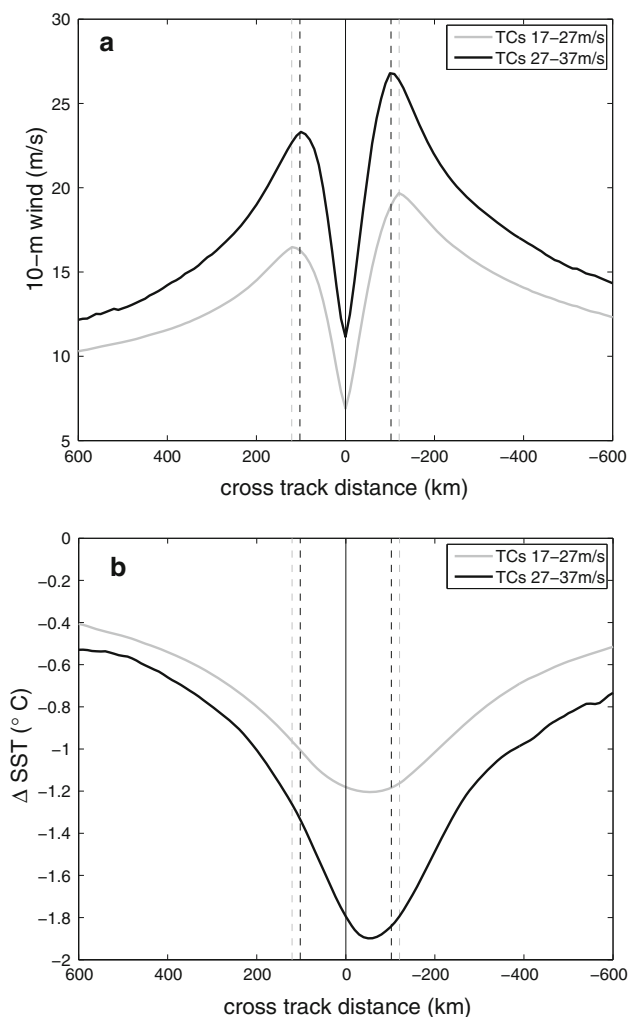


Fig. 7 Cross track composite of TC surface features: **a** 10-m wind speed (m s^{-1}) at TC occurrence time; and **b** SST cooling ($^{\circ}\text{C}$) at the time of maximum cooling. The results are presented for two TC wind categories: 17–27 m s^{-1} (gray lines) and 27–37 m s^{-1} (black lines). The vertical dashed lines represent the averaged radius of maximum winds for each category

5 Coupling effect on cyclonic activity

5.1 Cyclogenesis geography

The spatial distribution of cyclogenesis in the coupled and forced simulations and in observational data for the 20-year period 1979–1999 is represented by probability density functions (PDFs; Fig. 5c, d), as in Jourdain et al. (2011). The observations are given by extracting the simulation domain [139.6°–200.0°E, 31.4°–1.6°S] and period (1979–1999) from the new South Pacific Enhanced Archive for Tropical Cyclones (SPEARTC) dataset from Diamond et al. (2012). SPEArTC was built using data from the International Best Tracks for Climate Stewardship (IBTrACS) project information, historical

data from numerous islands and a strict quality control of each track.

The coupled model cyclogenesis distribution appears in very good agreement with observations and outperforms the forced model showing excessive cyclogenesis in the Coral Sea and in southeastern SPCZ region. The average number of cyclogenesis per year (Table 2) is also slightly overestimated in the forced model with 8.7 TCs/year compared with the observed 7.4 TCs/year that is closer to the coupled model result of 7.9 TCs/year. To better quantify the PDF differences, we partitioned the cyclogenesis distribution between western and eastern SPCZ regions, i.e., the Coral Sea and warmpool genesis areas, using the 170°E meridian as a separation line. Table 2 confirms the realistic east-west genesis distribution of the coupled model with 4.8 TCs/year in the Coral Sea and 3.1 TCs/year in the warmpool, very close to the observed 4.5 and 2.9 TCs/year respectively. The forced model produces about one more TC in the Coral Sea. This statistically significant difference (significant at 62 %) cannot be related to the large-scale atmospheric conditions as the CYGP distribution (Fig. 5a, b) is very similar in both simulations. It thus has to do with ocean-storm coupling whose mechanisms will be explored in Sect. 6.

5.2 Intensity distribution

The storm intensity distribution presented in Fig. 8 is the number of cyclone days per year as a function of central pressure. It shows that the coupled model succeeds in representing the intensity of intermediate-strength cyclones and poorly performs for the most intense ones. This is understandable considering the 35-km model resolution that smooths out the sharp eyewall structure of tangential winds; it also underestimates the strongest eyewall updrafts and compensating subsidence within the eye which contributes to the warming of the core region and hydrostatic reduction of central pressure (Gentry and Lackmann 2010). Extreme events in terms of intensity are thus missing in our simulations but they are rare and not statistically relevant to the impact of TCs on the ocean (Jullien et al. 2012) and feedback. On the other hand, the model overestimation of the lowest TC category of 1,000–1,010 hPa (Fig. 8) can be attributed to a shift in the intensity distribution of simulated cyclones as a consequence of coarse model resolution. More importantly for our coupling study, only the intensity distribution of the forced model overestimates the intermediate TC category of 970–990 hPa. This result can only be explained by the absence of negative SST feedback.

Interestingly, stronger TCs are more affected by the coupling process (Table 3). Towards the spectrum tail, TCs of category 4 are present in the forced model but absent in

Table 2 TC statistics from SPEArTC observations and from the forced and coupled models: annual mean and standard deviation of the number of cyclogenesis events; west/east distribution (i.e., Coral Sea/Warm Pool) of the annual mean; and mean TC life time of weak (17–27 m s⁻¹) and strong (27–37 m s⁻¹) cyclone categories

	Observations SPEArTC	Forced model	Coupled model
Number of TCs/year	7.4 ± 3.0	8.7 ± 3.1	7.9 ± 2.4
West/East distribution	4.5/2.9	5.7/2.9	4.8/3.1
Weak TC life time (days)	6.6	5.6	5.7
Strong TC life time (days)	8.2	8.8	7.8

the coupled model. On the contrary, weaker cyclones are only weakly affected by coupling. For quantitative analysis, the classification based on 2 categories of cyclones is justified: a moderate category with wind speed between 17 and 27 m s⁻¹ that features moderate coupling effects; and a category of strong TCs with winds over 27 m s⁻¹ that shows the largest effect.

6 Coupling effect on air–sea fluxes

6.1 SST cooling

The composited effect of TC occurrence on SST and air–sea fluxes is examined as a function of time relative to TC passage (lag) where a zero lag represents the occurrence time. As described in Sect. 2.6, this Eulerian composite is a 400-km cross-track average at each TC location. A comparable composite is constructed for microwave SST observations from the Tropical Rainfall

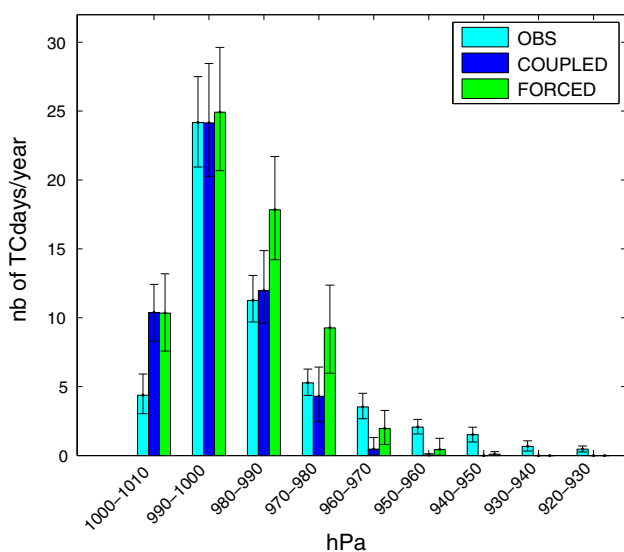


Fig. 8 Distribution of TC central pressure (in number of TC days per year) for the period 1979–1999 and from SPEArTC observations (cyan), the coupled model (blue) and the forced model (green). The 5–95 percentiles bootstrap error bars are also presented

Table 3 Percentage of the difference in TC days between forced and coupled models in various storm categories

TC pressure category (hPa)	Coupling effect on TC events (%)
1,000–1,010	–25
990–1,000	–24
980–990	18
970–980	36
960–970	67
950–960	90
940–950	100

Measuring Mission (TRMM) Microwave Imager (TMI) and Advanced Microwave Scanning Radiometer for Earth Observing System (AMSR-E; <http://www.ssmi.com/sst>). Microwave SSTs are taken from 1998 to 2007 along the observed cyclone tracks. Cooling is defined as the difference between local SST and pre-storm (ambient) SST. Ambient SST is computed as the averaged value between days –10 and –2 as in Jullien et al. (2012). For both model and observations, the seasonal SST cycle is removed by subtracting the daily climatology.

The mean Eulerian representation of TC-induced cooling is shown in Fig. 9 for the coupled model and TMI-AMSR-E observations. The coupled model shows a realistic depiction of cooling intensity and timing. The maximum SST cooling occurs 2 days after passage of the storm center because of the time needed by upwelling and near-inertial mixing to impact surface temperatures (Jullien et al. 2012).

6.2 Specific humidity

The evolution of 2-m specific humidity (Fig. 9b, black curves) shows little differences between coupled and forced simulations with, in both cases, an increase of humidity during cyclone occurrence. The storm impact is noted from days –5 to +5 because of its very large spatial extent. The difference between the two runs can be attributed to a small difference in large-scale conditions and in storm intensity associated with a few stronger (Fig. 9b, red curves) and moister TCs in the forced simulation.

Sea level specific humidity (Fig. 9b, blue curves), on the other hand, is significantly different between the two simulations because it is tightly related to SST. In the forced run, there is no cooling feedback and sea-level humidity only slightly increases during cyclone occurrence because of the warm core low pressure anomaly. The reduction of surface pressure is one known process that affects surface fluxes by increasing the saturation mixing ratio (e.g., Schade 2000). In the coupled simulation however, humidity changes are opposite and much larger than

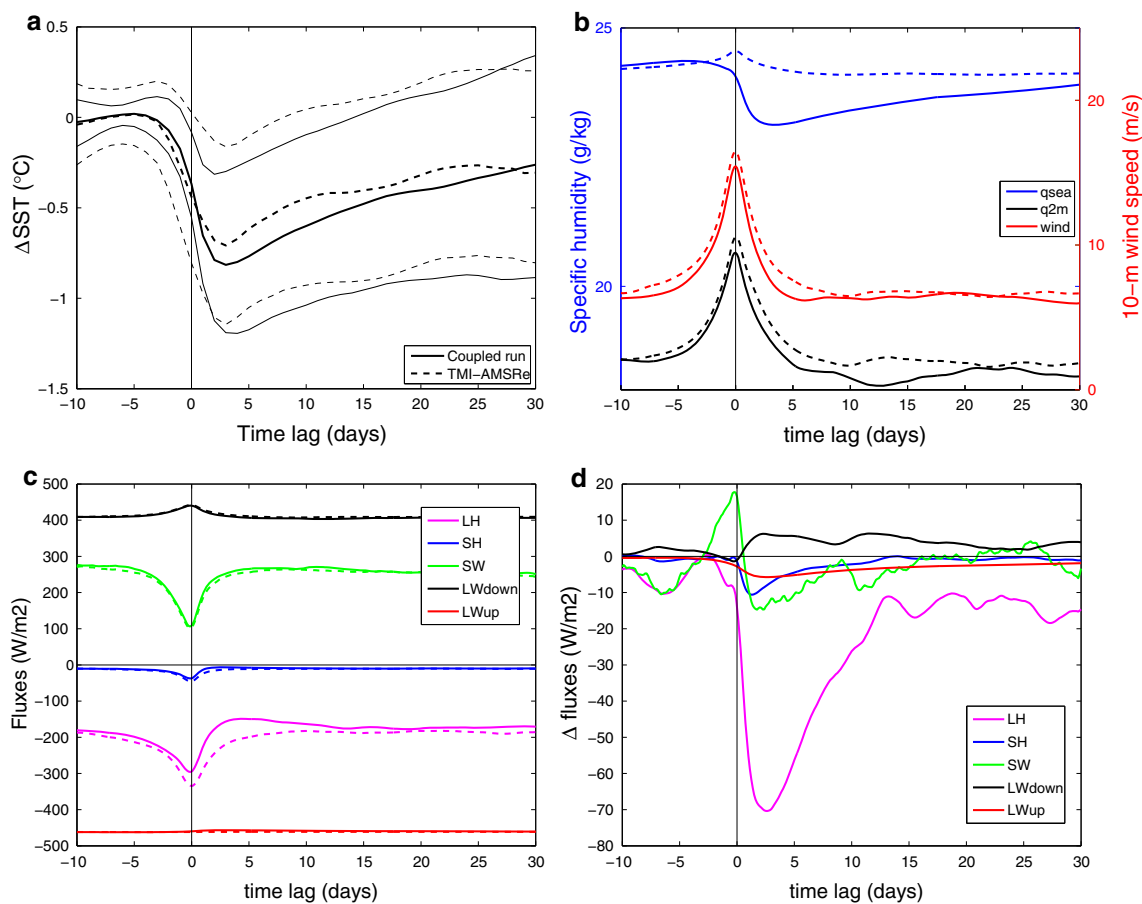


Fig. 9 Cyclone wake composites as a function of time from TC occurrence (lag in days). **a** SST cooling ($^{\circ}\text{C}$, bold lines) and its standard deviation (thin lines) for the coupled model (solid lines) and TMI-AMSR observations (dashed lines); **b** 10-m wind speed (m s^{-1} , red lines) and specific humidity (g kg^{-1}) at 2 m (black lines) and at sea level (blue lines) in the coupled model (solid lines) and forced

model (dashed lines); **c** surface heat fluxes in the coupled model (solid lines) and forced model (dashed lines); and **d** the surface flux difference between forced and coupled models. Latent heat flux is in purple, sensible heat flux in blue, shortwave radiation in green, longwave downward radiation in black and longwave upward radiation in red

those created by pressure changes. Sea level specific humidity follows the evolution of surface cooling with a maximum decrease 2 days after TC passage. This leads to a reduction of air–sea moisture difference, i.e., the thermodynamic disequilibrium at the sea surface that weakens the latent heat flux.

6.3 Air–sea fluxes

The evolution of air–sea fluxes as the cyclone passes are presented in Fig. 9c. Short-wave radiation to the ocean decreases during TC occurrence because of TC clouds that limit the penetration of downward solar fluxes in the troposphere. On the contrary, downward long-wave radiation increases because of TC clouds, but at a lower rate. Sensible and latent heat fluxes from the ocean to the atmosphere both increase when storm winds extract heat and moisture from the ocean, the latent heat flux being largely

dominant. The difference between forced and coupled simulations is also most important for the latent heat flux (Fig. 9c, d). There is a milder effect on the sensible and upward long-wave radiation. The latter is directly affected by SST cooling and thus follows the same evolution pattern with a maximum decrease of 5 W m^{-2} 2 days after TC passage. The decrease in sensible heat flux of 10 W m^{-2} can be attributed to both SST cooling and a decrease in wind intensity in the coupled simulation. More importantly, the latent heat flux is 70 W m^{-2} lower in the TCs of the coupled simulation following cyclone occurrence. This can be attributed to some extent to the presence of weaker cyclones in the coupled run but the time evolution of changes with a peak 2 days after TC passage rather suggests a major effect of SST cooling through its control of sea-level specific humidity. The mean effect of ocean–hurricane coupling is thus an SST cooling of $0.6 \text{ }^{\circ}\text{C}$ (Fig. 9a) that leads to a latent heat flux reduction of

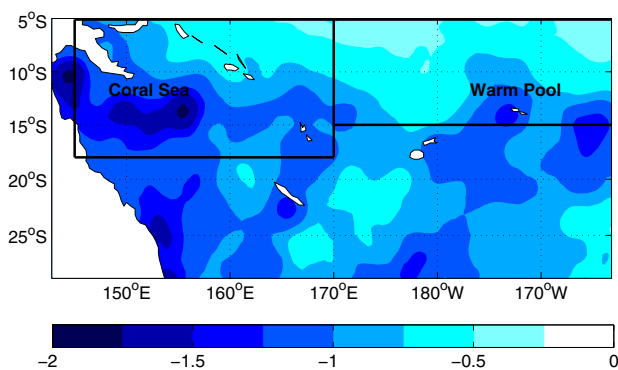


Fig. 10 Composite map of storm-induced SST cooling ($^{\circ}\text{C}$). In the construction of this map, if two TC tracks overlap, the coolings are averaged

70 W m^{-2} and a lesser reduction in sensible heat flux of 10 W m^{-2} .

7 The role of ocean dynamics

7.1 Geography of storm-induced cooling

Ambient SST and TC-induced SST cooling are both related to the ocean stratification, which is structured by ocean dynamics. At the regional scale, stratification in the Coral Sea is strongly affected by negative winter heat fluxes and downwelling associated with the gyre-scale anticyclonic circulation (Marchesiello et al. 2010). The winter mixed layer is deep and relatively cold, contrasting with the warm pool region characterized by a thick layer of warm water piled up by equatorial currents. Summer stratification in the Coral Sea then produces a shallow layer of warm water above the cool water generated in winter. The potential for storm-induced SST cooling is thus particularly high in the Coral Sea and low in the warm pool.

This is confirmed by our experiments. A map representing the combined SST cooling of all TCs over the 20 years of coupled simulation is presented in Fig. 10. It is computed by mapping all SST cooling events along TC tracks and taking the average value of 2 events if there tracks happen to cross each other. This map provides a distribution of TC-induced cooling in the southwest Pacific that confirms strong cooling in the Coral Sea where the oceanic mixed layer is relatively shallow (Fig. 4a, b). On the contrary, very weak cooling appears in the warm pool.

7.2 Storm sensitivity to SST

To isolate the SST feedback effect in the relation between central pressure and SST, we now present (Fig. 11a) the TC intensity difference between forced and coupled runs as

a function of ambient SST and SST cooling.³ Here, SST cooling is not defined as the maximum found in the TC area but as the mean inner-core value (averaged over 400 km cross track), which should be more relevant to the feedback effect. Large negative values of pressure difference (red color in Fig. 11a) indicates strong coupling effect (SST feedback). A maximum reduction of 15 hPa in central pressure occurs for SST cooling of 2°C and ambient SST of more than 28°C . Figure 11a shows that storm intensity is affected by both SST effects but is more sensitive to TC-induced cooling than to ambient SST. Interestingly, the maximum possible SST cooling calculated by Schade 2000, cooling that results in the cancellation of radial gradient of moist entropy in the boundary layer, is also present in our modeling results and increases with the ambient SST as predicted (see the white area of Fig. 11a where TCs would be suppressed by excess cooling).

An indication of coupling sensitivity to SST cooling alone can be obtained by averaging the previous functions for all ambient SST categories (Fig. 11b). It shows that the feedback effect on storm intensity is highly nonlinear. It is weak for coolings below $1\text{--}1.5^{\circ}\text{C}$ but then increases steadily at a rate of about $15 \text{ hPa }^{\circ}\text{C}^{-1}$. Even for strong cooling, the intensity feedback is less than half the theoretical range given by Holland (1997) and Schade (2000) but closer to that of idealized and test case experiments (Table 1).

7.3 Mixed layer depth

Instead of SST cooling, Wu et al. (2007) have used the ambient MLD as a parameter of oceanic feedback. It provides a more easily measurable quantity for prediction of storm intensity. In our realistic experimental setting, the variability of storm intensity for any given MLD value (due to the variability of atmospheric conditions or intrinsic processes) renders the comparison between forced and coupled models quite sensitive. Akin to a binning method, we selected comparable TCs by entering SST cooling as a binning parameter. The SST cooling bins can assemble events of comparable intensities (reducing the risk that coupled and forced TCs are incomparable in the parameter space). Then, averaging all SST cooling categories for each MLD bin provides a sensitivity value to ambient MLD alone (Fig. 11c).

This estimation has again a nonlinear behavior: it is low for deep MLD but for shallower MLD it reaches 5 hPa

³ To generate the SST cooling associated with TCs of the forced atmospheric simulation, we ran the ocean model alone driven by surface fluxes from the forced atmospheric model. This forced oceanic simulation (without SST feedback to the atmosphere) gives the oceanic response to the forced atmospheric model, which can be compared to the fully coupled model response.

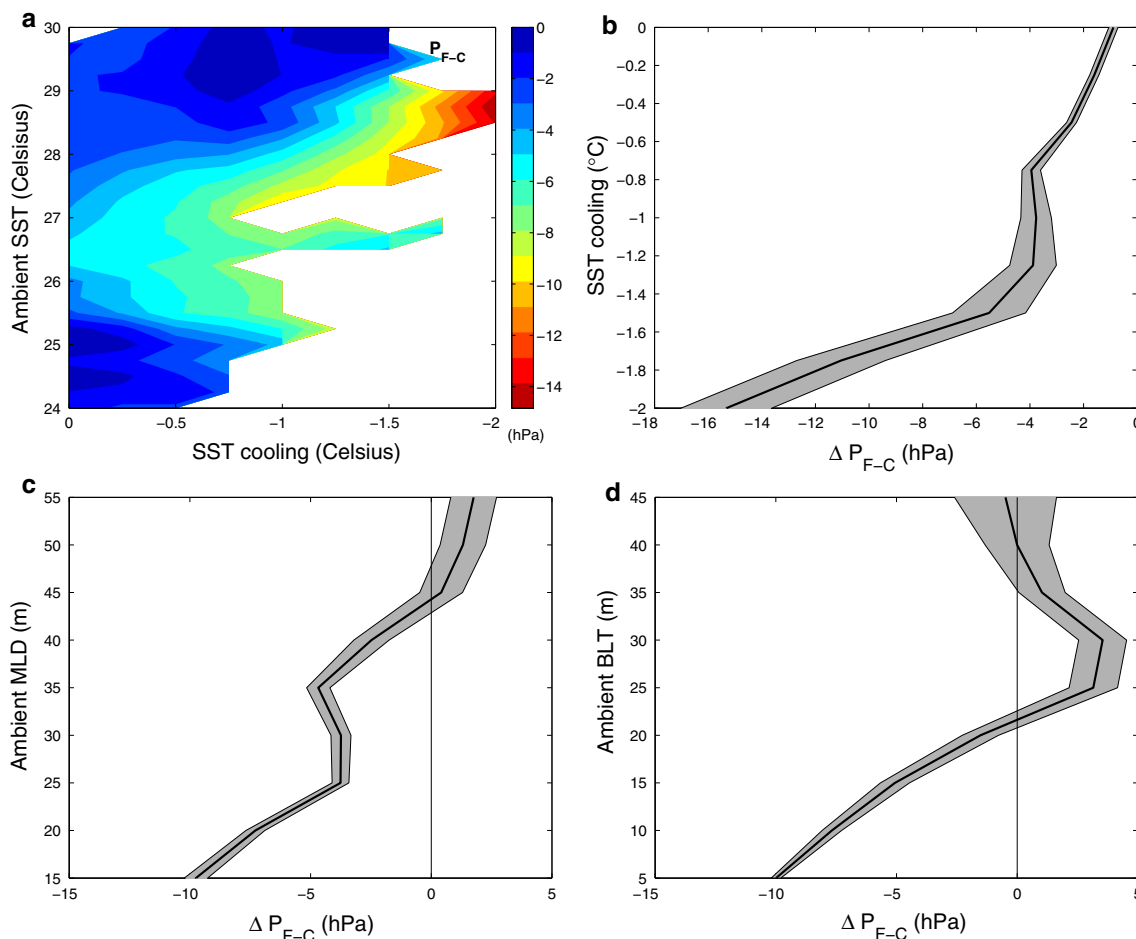


Fig. 11 TC central pressure difference (hPa) between forced and coupled models as a function of **a** SST cooling and ambient SST; **b** SST cooling; **c** ambient MLD; and **d** ambient BLT. The standard error of the mean (at 90 % confidence) is presented in shades of grey in (b–c–d)

increase of TC central pressure for every 10 m increase of MLD (compare with a constant value of 4.7 hPa/10 m given by the simple model of Wu et al. 2007). There are uncertainties associated with the methodology but our results are consistent with the expectation that entrainment of cold subsurface water should be weakly sensitive to deep mixed layers (at least for depths deeper than the mixing length due to extreme winds). The analysis is also consistent with our previous observation that variations of MLD between the Coral Sea and warm pool regions are correlated with the differences in SST cooling and negative feedback effects.

7.4 Barrier layers

Balaguru et al. (2012) and Neetu et al. (2012) recently suggested that the salinity barrier layer of tropical oceans may be another key player in the SST cooling process that impacts storm intensity. A barrier layer between the oceanic mixed layer and the underlying thermocline occurs when enough fresh water pours into the ocean from strong

tropical precipitation (subduction of salty water from eastern equatorial regions is another contributor). Depending on its thickness, it can insulate the surface from subsurface colder waters. The model and observed summer climatological distribution of barrier layer thickness (BLT) are presented in Fig. 4c, d. It shows that a barrier layer is only present in the SPCZ and warm pool regions but large thickness values are characteristic of the warm pool. The fact that thick barrier layers tend to be also located in areas of deep mixed layers could weaken arguments based on the correlation between storm intensity and BLT. To test the robustness of our results, we sub-sampled the modeled TC tracks following various criteria: ambient SST (as in Balaguru et al. 2012) above 28 °C; shallow MLD; or, contrariwise, deep MLD. In all cases, the coupling sensitivity to BLT is similar to that presented in Fig. 11d. Figure 11d indicates that a critical thickness exists (around 25 m) beyond which storm-induced cooling and feedback are prevented. Below 25 m thickness, storm intensity is sensitive to BLT at a rate of about 5 hPa increase of TC central pressure for every 10 m increase of BLT.

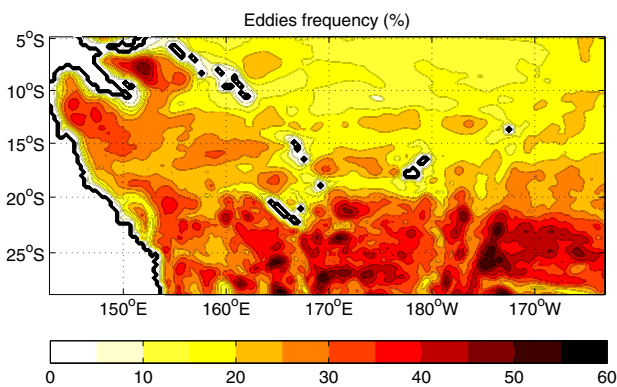


Fig. 12 Eddy frequency as the percentage of eddy presence in the 1979–1999 coupled model

7.5 Ocean eddies

The effect of mesoscale eddies in the feedback mechanism of storm intensity has been mostly studied in the Gulf of Mexico (e.g., Bao et al. 2000) or in the North Pacific (Wu et al. 2007; Zheng et al. 2010) where loop currents frequently release large eddies, sometimes along cyclone tracks. As yet, no reported attempt has been made to provide global statistical estimations of ocean eddies effect on storm intensity. Our experimental design allows us to provide basin-scale estimates.

We tracked all ocean mesoscale eddies of the computational domain using the tracker methodology described in Chaigneau et al. (2008, 2009) and constructed composite plots of coupling effect on TCs crossing cyclonic or anticyclonic eddies. The cyclonic (anticyclonic) eddy detection algorithm consists in locating eddy centers associated with local minima (maxima) of sea level anomaly (SLA) in a moving window of 6×6 grid points. Then, for each possible eddy center, the algorithm searches for the outermost closed SLA contour, which corresponds to the eddy edge. For each identified eddy, the apparent eddy radius corresponds to that of an equivalent circular vortex of the same area.

Mesoscale eddies in the southwest Pacific are associated with zonal jets driven by particularly numerous islands and ridges of this part of the world (Couvelard et al. 2008). The eddy field can be separated in two large families located to the north and south of New Caledonia (Fig. 12). In the North, eddies are mostly confined to the Coral Sea and are generated by barotropic instability of the North Caledonia and Vanuatu jets. In subtropical latitudes between 20° – 30° S, there is a zonal band of numerous strong eddies associated with baroclinic instability of the South Pacific Subtropical Countercurrent Qiu et al. (2008). A number of eddy generation are also associated with western boundary currents (East Australian and North Queensland currents) closer to Australia. On the contrary, the warm pool region is a desert in terms of mesoscale eddies.

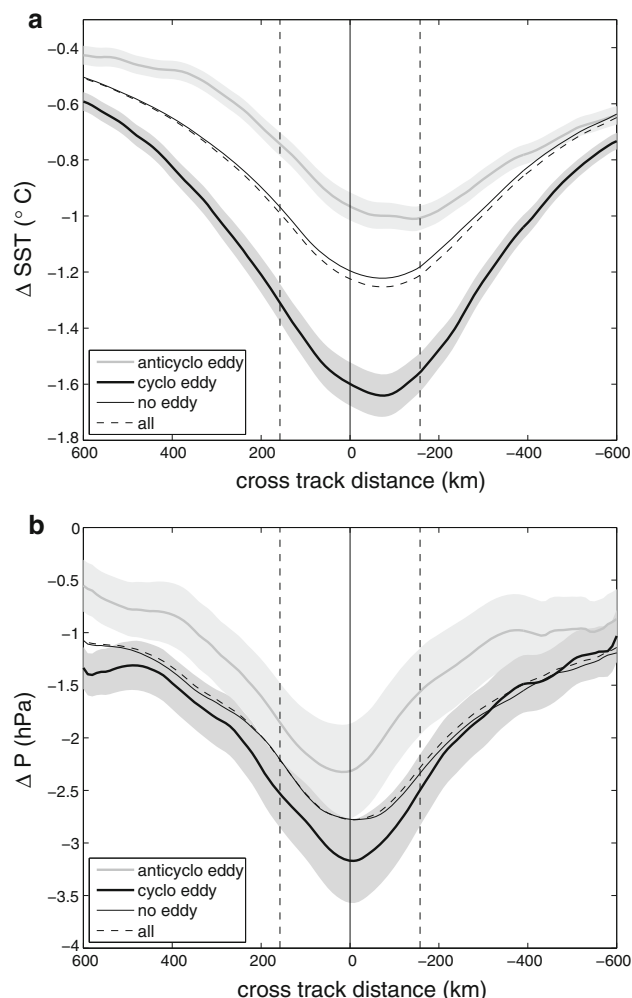


Fig. 13 Cross track composites of **a** SST cooling ($^\circ\text{C}$) in the coupled model and **b** TC central pressure differences (hPa) between forced and coupled models. The results are given for all TCs (*dashed line*); TCs located over a cyclonic eddy (*bold black solid line*); TCs located over an anticyclonic eddy (*bold gray solid line*); TCs located over a neutral ocean (neither a cyclonic nor anticyclonic eddy; *thin black solid line*). The standard error of the mean (at 90 % confidence) is presented in *shades of grey*

Figure 13 presents a cross-track composite (Sect. 2.6) of SST cooling and associated central pressure difference between forced and coupled runs for TCs positioned over pre-existing cyclonic or anticyclonic ocean eddies. The same analysis is given for TCs positioned over a neutral area (no underlying eddies, which represents the most frequent condition: 80 % of the time) and for all TCs combined. TCs cross over cyclonic eddies more frequently (11 % of the time) than anticyclonic eddies (9 % of the time) because there are simply more cyclonic eddies. Anticyclonic eddies are characterized by a deepened mixed layer and clearly appear to limit SST cooling compared to the general case by providing an insulating effect against storm-induced upwelling and mixing. Cyclonic eddies on

Table 4 Ocean mixed layer heat budget (integrated from day -10 to the time of maximum cooling) under TCs as they cross over cyclonic and anticyclonic eddies ($^{\circ}\text{C}$)

	Rate	Vmix	Vadv	Hadv	Forc	Hmix	Entr
Cyclonic eddies	-1.55	-0.23	-1.03	0.18	-0.72	-0.02	0.26
Anticyclonic eddies	-0.85	-0.06	-0.45	0.11	-0.69	-0.01	0.26

The budget terms are: Rate, the time rate of change; Vmix, vertical mixing; Vadv, vertical advection; Hadv, horizontal advection; Forc, surface forcing; Hmix, horizontal mixing; and Entr, entrainment

the other hand are characterized by shallower mixed layer and tend to promote particularly strong cooling.

An interesting feature is that cooling over cyclonic eddies is less asymmetric, due to a larger part played by upwelling compared to mixing, as indicated by the surface heat budget analysis presented in Table 4 (see Jullien et al. 2012 for the exact definition of all terms). TC-induced upwelling is a deep process that occurs under the cyclone eye and produces vertical advection towards the mixed layer base (Jullien et al. 2012). TC-induced mixing is a relay process of upwelling as it brings subsurface water up to the surface, but it is asymmetric with respect to the cyclone eye. In the case of anticyclonic eddies, the asymmetric effect is increased because the relay is rendered more difficult by mixed layer deepening (upwelling is limited to deeper levels). On the contrary for cyclonic eddies, the relay is almost as efficient in the cyclone eye as on the strong cyclone side because upwelling reaches shallower levels. Overall, eddies slightly increase storm-induced cooling compared to the neutral case (albeit not significantly so), because cyclonic eddies are slightly more frequent than anticyclonic eddies and also because the cooling tendency of cyclonic eddies is larger than its limitation by anticyclonic eddies.

The eddy feedback effect on storm intensity is consistent with the cooling patterns, showing a significant decrease (increase) of central pressure for TCs crossing over anticyclonic (cyclonic) eddies. The amplitude of central pressure anomalies is relatively small (about $2 \text{ hPa } ^{\circ}\text{C}^{-1}$). Recall that the largest sensitivity of storm intensity to SST cooling is highly nonlinear showing significant values only for strong coolings associated with strong TCs ($15 \text{ hPa } ^{\circ}\text{C}^{-1}$). Here, the sensitivity to eddy effects is given for all combined TCs, which are considerably more numerous in the weak categories. The sensitivity for stronger TCs is thus expected to be much larger but the signal to noise ratio decreases for extreme events.

8 TC intensification

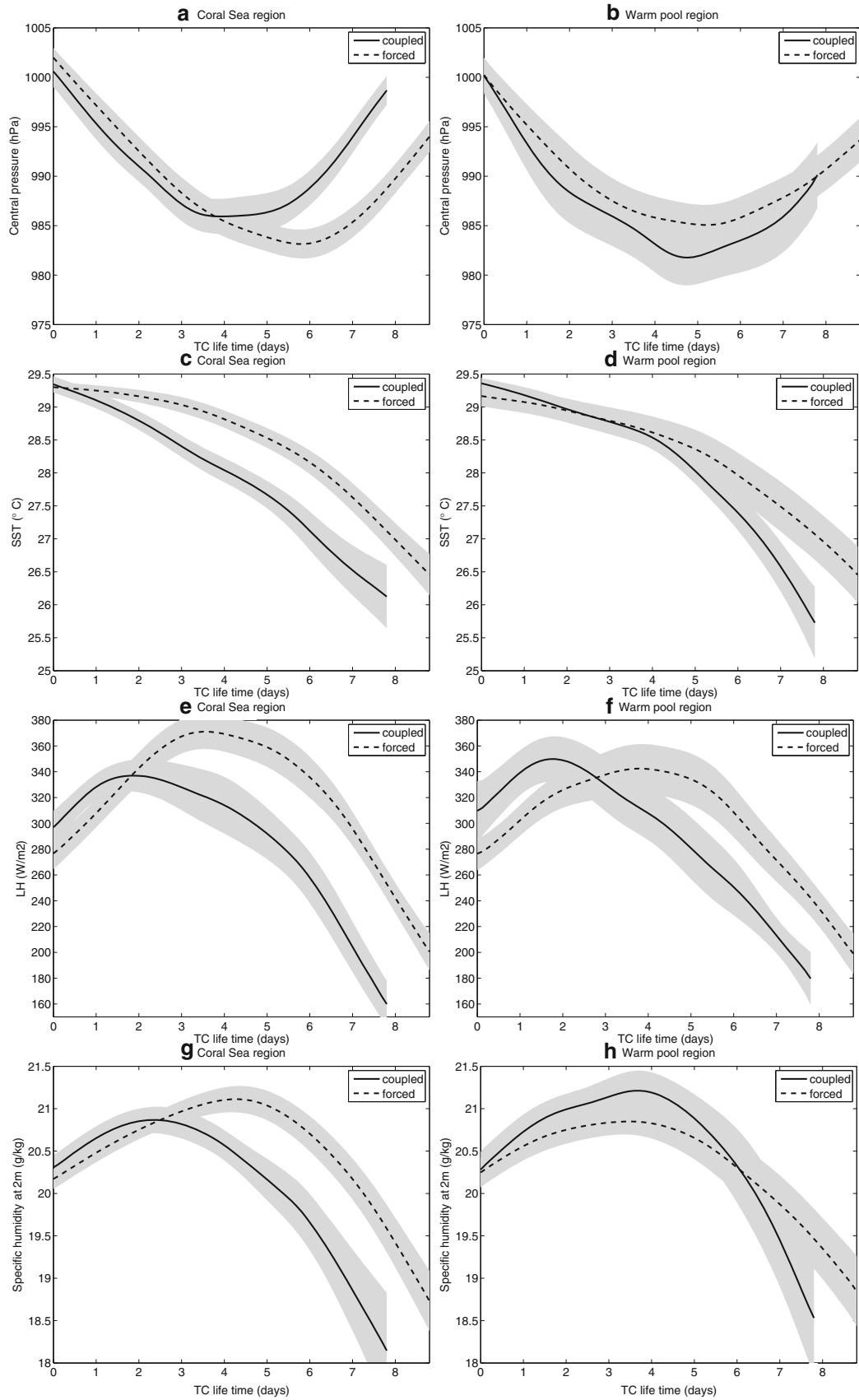
Finally, we investigate the evolution of TCs along their track, i.e., their life cycle of initialization, intensification,

maturity and decay phases. For simplicity, we only consider strong TCs ($>27 \text{ m s}^{-1}$), and two regions of interest: the Coral Sea region in the west characterized by shallow oceanic mixed layer and the warm pool region in the northeast with warmer SST and deeper oceanic mixed layer. The life cycle of moderate cyclones is similar in the coupled and forced simulations and in both regions. However for strong TCs, there is a clear regional modulation. Note that coupled TCs have a shorter lifetime in average (strong TCs) than forced ones: 7.8 days instead of 8.8 days compared with 8.2 days in the observations (see Table 2). In Fig. 14, the lifetime of forced and coupled TC composites are rescaled according to their respective mean values.

The composite cyclone evolution along its track (Sect. 2.6) is first illustrated by its central pressure in Fig. 14a, b. In the Coral Sea, the forced composited cyclone can reach higher intensity, while in the warm pool region, forced and coupled models experience similar TC evolution.

SST evolution (Fig. 14c, d) shows continuous cooling along the composite cyclone tracks, illustrating the general southward storm migration where ambient water becomes increasingly cold. In the Coral Sea, cooling by strong TCs adds up to the change of ambient SST, limiting the intensification process in the coupled model. In the warm pool region, coupled cyclogenesis occurs on warmer waters and the along-track cooling rate is weaker during the intensification phase than in the Coral Sea. These two features lead to a greater supply of latent heat to the intensifying cyclone (Fig. 14f) and thus act as a natural selection process for maintaining the presence of strong coupled cyclones. Note that the latent heat supply rapidly falls down because of TC migration to colder waters and TC-induced SST cooling (Fig. 14c–f).

These results are indicative of the factors that control the rate of intensification in the model. Even though latent heat supply from warm waters are needed for cyclogenesis, storm evolution from intensification to mature and decaying phases is uncorrelated with instantaneous SST and surface heat flux, even in the forced model. SST decreases continuously during the intensification process and the decrease of latent heat flux starts two days before the decaying process. Therefore, tropical cyclones are not adjusted to the inner core surface fluxes, contrarily to the assumption made in



◀ **Fig. 14** TC life cycle composite constructed from 400-km cross-track averages of TC characteristics in the forced and coupled models. Only strong TCs with wind speed $>27 \text{ m s}^{-1}$ are considered. **a, b** TC central pressure (hPa); **c, d** SST ($^{\circ}\text{C}$); **e, f** latent heat flux (W m^{-2}); **g, h** specific humidity at 2 m (g kg^{-1}). The results are for the Coral Sea region on the *left* and warm pool region on the *right*. *Dashed (solid) curves* are for the forced (coupled) model. The standard error of the mean (at 90 % confidence) is presented in *shades of grey*

thermodynamic paradigms of TC intensification. This findings are consistent with the idealized experiment presented by Montgomery et al. (2009). Using both mesoscale and cloud-scale atmospheric models, the authors investigate the sensitivity of vortex intensification by capping the wind speed effect on latent and sensible heat fluxes in the bulk-aerodynamic formulae (i.e., surface fluxes are unaffected by wind speed past a certain threshold). In this case, the WISHE instability mechanisms involving mutual feedback between surface fluxes and tangential velocity in the core region is shut down. Yet, final storm intensity is only weakly modified and the characteristics of vortex evolution are otherwise unaffected. Smith et al. (2009) in a companion paper show that vortex spin-up is largely controlled by frictional convergence that has the dual role of moistening the core region (providing latent heat to the warm core aloft) and increasing tangential winds by conserving absolute angular momentum (the dynamical role of the boundary layer). They conclude that surface fluxes affect the final storm intensity but are unessential to the instability mechanism. In our case also, the along-track decrease of ambient SST and storm-induced cooling reduces the final storm intensity but poorly affects its evolution pattern. On the contrary, both inner-core surface humidity (Fig. 14g, h) and humidity convergence (not shown) are correlated with storm intensity.

Following Wada (2009), we computed the time accumulation of surface heat fluxes (Fig. 15), a measure of the accumulated upper-ocean heat content transported in the eyewall and released in the adiabatic heating process. It shows a much better relation with the timing of coupling effect. The cut-off point where the coupled model accumulated heat flux is lower than that of the forced model corresponds to a change in storm intensity between the two simulations. In the Coral Sea, this point is between day 2 and 3 and nearly coincides with the moment when intensification shows the effect of coupling; in the warm pool, it lies in the decaying phase at day 6. In all cases, coupled cyclones decay faster than forced ones (explaining the mean difference in life duration) but the secondary circulation appears as a mediator of storm reaction to changes in surface fluxes.

All that supports the notion that the evaporation-wind feedback process is not essential to intensification, implying delayed SST effect on storm intensity. It would explain that realistic model applications tend to produce lower SST

feedback effects than predicted from thermodynamic and gradient-wind balance assumptions alone.

9 Summary and discussion

In this study, we present and analyze the first long-term, regional coupled simulation of the South Pacific cyclonic activity. The coupled modeling system is state-of-the-art and applied for mesoscale resolution (35 km grid mesh size). 20 years of simulation (1979–1999) and about 160 tropical cyclones provide some statistical reliability that is generally missing in event studies. The modeled cyclonic activity is characterized by its environmental conditions, by the structure of TCs, their spatial and intensity distributions, and air–sea exchanges that control their intensity.

We first checked the model skills in reproducing the observed regional atmospheric and oceanic climate, in particular the SPCZ position generally poorly represented in global models. The model was also shown to produce realistic tropical cyclones and magnitude of storm-induced surface cooling. This validation stage allowed us to proceed with the statistical analysis of TC–ocean interaction in the South Pacific.

The environmental conditions of cyclogenesis evaluated with the CYGP genesis index gives a stronger probability of cyclogenesis in the Coral Sea region. Cyclogenesis distribution in the forced simulation closely follows the CYGP pattern but the coupled model solution is closer to the observed distribution where cyclogenesis spreads further eastward in the warm pool area. This is the first reported evidence of air–sea coupling impact on cyclogenesis spatial distribution. It indicates that cyclogenesis indices must account for subsurface ocean features (not only SST) for proper prediction. The intensity distribution and average number of TCs is also better represented in the coupled than in the forced model arguing again for a significant role played by oceanic feedback on cyclonic activity. This feedback effect increases with storm intensity.

The composite study of coupling mechanisms revealed that storm-induced SST cooling leads to a mean decrease in air–sea fluxes of 70 W m^{-2} for the latent heat flux, 10 W m^{-2} for the sensible heat flux and 5 W m^{-2} for long-wave upward radiation. Ocean dynamics at multiple scales are able to modulate these numbers by their control of surface stratification. The shallow MLD of the Coral Sea associated with the regional anticyclonic gyre circulation is favorable to strong SST cooling and negative feedback effect on storm intensity. On the other hand, the thickness of salinity barrier layers in the warm pool is a limiting factor of storm-induced SST cooling and thus promote TC intensification. Even mesoscale ocean eddies that are mostly generated in the Coral Sea (as opposed to the warm

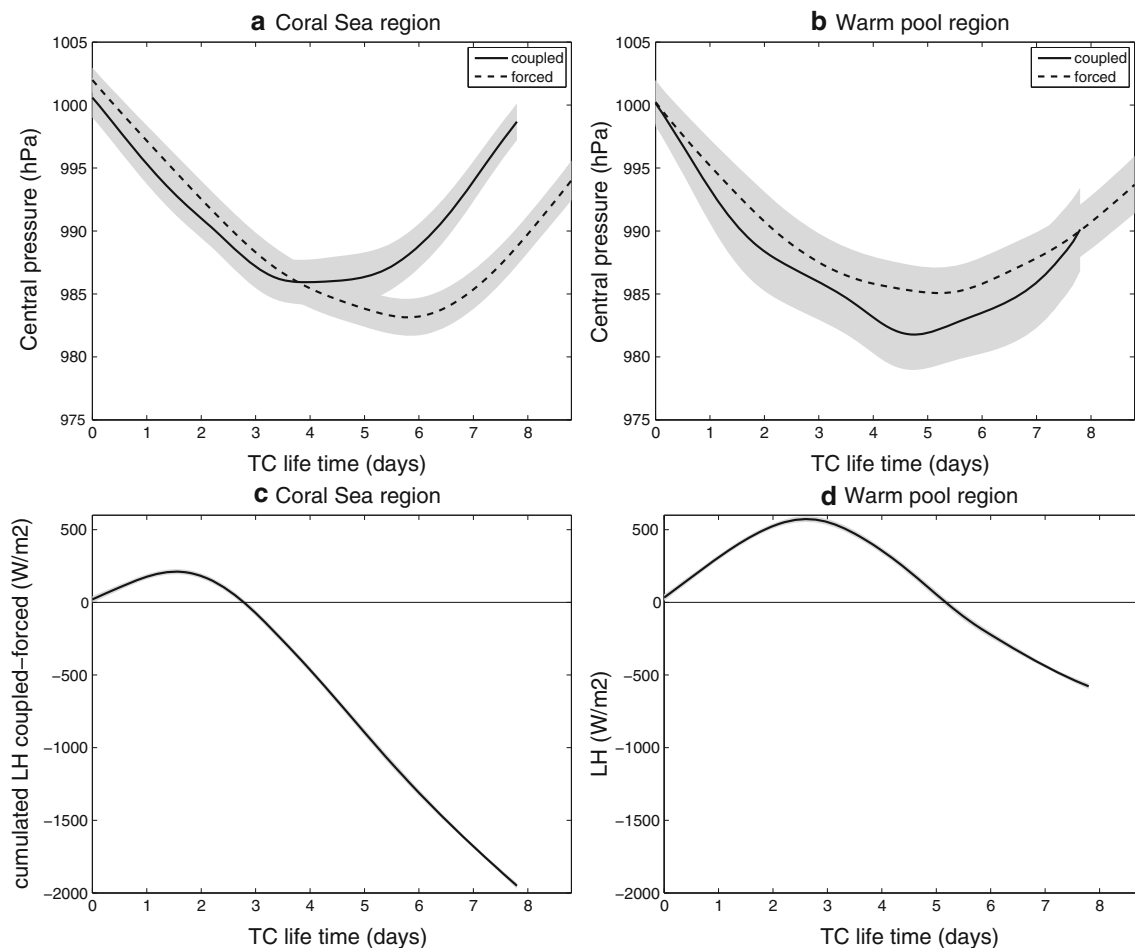


Fig. 15 Same as Fig. 14 for **a, b** TC central pressure (hPa); **c, d** cumulated latent heat flux difference (W m^{-2}) between coupled and forced models

pool) may have a residual negative effect that would accentuate the regional differences between the two regions. These environmental factors all contribute to spread the cyclogenesis distribution eastward by limiting the recruitment of TCs in the Coral Sea (from the large pool of mesoscale vortices) and to restrict intensification of the strongest storms.

Our results quantify the sensitivity of storm intensity to SST cooling. It is highly nonlinear, i.e., weak for weak SST cooling and about $15 \text{ hPa } ^\circ\text{C}^{-1}$ for strong cooling above 1°C . These numbers are in the range of previous realistic case studies (Table 1; Bender et al. 1993; Bender and Ginis 2000), but much lower than theoretical estimations (Table 1; Holland 1997; Schade 2000). The difference may be understood through the paradigms proposed for TC intensification. The underlying paradigm behind theoretical estimations of SST feedback effects is the evaporation-wind feedback process (WISHE; Emanuel 1986). WISHE requires that storm intensity be directly restricted by the magnitude of surface heat and moisture fluxes in the core

region (Craig and Gray 1996). The axisymmetric model of Emanuel (1986) assumed gradient-wind and hydrostatic balance everywhere, thus precluding unbalanced dynamics such as radial convergence in the lower troposphere and boundary layer (predicted by the Sawyer-Eliassen equation of secondary circulation). Our results contradict this paradigm by showing a lack of correlation between storm intensification and surface fluxes. This is similar to the experiment of vortex evolution with capped fluxes (Montgomery et al. 2009). The effect of SST is thus not instantaneous but accumulated over time within the inner core of the cyclone. Macro-scale processes, particularly the role of radial advection in the boundary layer and lower free troposphere must be accounted for (Smith et al. 2009).

Radial convergence has a dual role in moistening the core region and increasing its tangential speed through absolute angular momentum conservation (Fig. 6f). Surface friction provides both an intense radial flow that fuels the storm engine and a competing dissipation mechanism. Further studies should thus focus more importantly in the

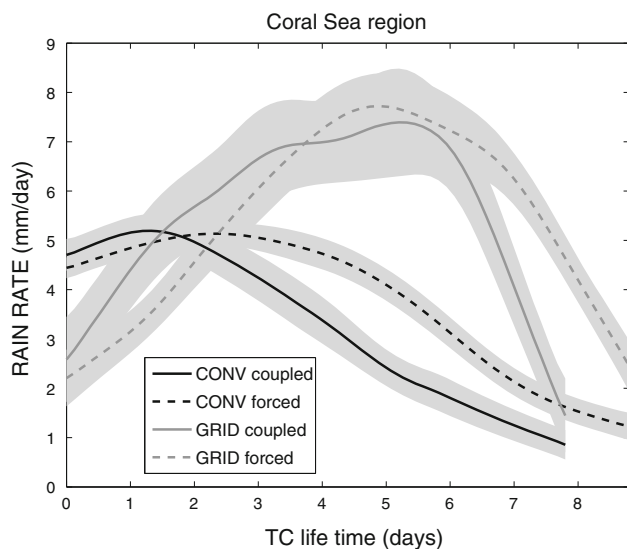


Fig. 16 TC life cycle composite for subgrid-scale (CONV) and grid-scale (GRID) precipitations (mm day^{-1}) in the coupled and forced models and in the Coral Sea for TCs with wind speed $>27 \text{ m s}^{-1}$. The standard error of the mean (at 90 % confidence) is presented in shades of grey

parametrization of surface momentum fluxes and boundary layer dynamics (as also discussed in Nolan et al. 2009).

It is generally argued (see Craig and Gray 1996) that the choice of convection scheme in mesoscale models would determine the time scale of convection and thus the instability mechanisms for storm intensification. In our model, cumulus convection appears more affected by coupling than macro-scale circulation (Fig. 16). This is consistent with the work of Wada (2009) using a cloud-resolving model coupled with a slab mixed-layer ocean model. In cloud-resolving models, cumulus convection during the early intensification phase is organized as intense eyewall mesovortices. They play a crucial role in the vertical transfer of heat and moisture before merger and axisymmetrisation result in an annular ring of vorticity. Similarly to our findings, SST feedback in Wada (2009) is essentially effective against mesovortices (represented as sub-grid scale convective processes in our case) but has a poor effect on macro-scale dynamics. The author concludes that coupling effects are different at various stages of intensification. Interestingly, it is also the accumulation of upper-ocean heat content, not instantaneous surface fluxes, that affects TC intensity in this coupled cloud-resolving experiment.

In mesoscale models, it is conceivable that convection schemes with faster adjustment leading to more efficient adiabatic heating would increase the response of intensification rate to surface heat fluxes. We tested the Kain–Fritsch scheme (see Jourdain et al. 2011), which increases the ratio of subgrid- to grid-scale precipitation during TC

intensification. We found a general degradation of model results for both the large-scale conditions (SPCZ dynamics) and TC activity (largely overestimated cyclogenesis number). We thus believe that our original modeling setup provides the most realistic results.

Even though our model suggests a lower range of SST feedback effect than predicted by theory, this effect remains significant on the statistics of cyclonic activity. It confirms the suggestions made from idealized model or case studies that the negative feedback appears stronger for regions where intensity potential is larger, MLD is smaller, barrier layers are thinner or absent. Vincent et al. (2012b) propose a Cooling Inhibition index (CI) based on these multiple quantities. It is intended for evaluating the potential coupling impact on TC intensity, genesis and intensification rate. However, beyond the known effect on TC intensity, we show that coupling has also an effect on the yearly cyclogenesis number as more TCs are produced in the forced model. We suggest that among the large pool of mesoscale vortices generated during the cyclonic season in the SPCZ, even a small effect of SST feedback would impact the recruitment of named TCs.

Other characteristics of cyclonic activity appear less affected by SST feedback. The effect on storm tracks suggested by Bender et al. (1993) as a result of alteration of the beta drift (due to weakening of the tangential flow) is not apparent in our results. Specific analysis may be required to extract this information. There is a clear coupling effect, however, on the TC life time of strong events which is shorter in average in the coupled model and closer to observations (Table 2). On the effect of translation speed, as pointed out in Jullien et al. (2012), South Pacific TCs are generally fast moving storms with Froude numbers (ratio of TC translation speed to the first baroclinic mode phase speed of near-inertial oscillations) usually >1 (about 2 in the mean, corresponding to a mean TC translation speed of about 4 m s^{-1}). Low Fr numbers are accidental along cyclone tracks and their effect are embedded in the composites. The general effect of storm translation is to reduce SST cooling in the inner-core by about half its maximum value in the outer region. Therefore, the high maximum values of SST cooling (up to $5\text{--}6 \text{ }^\circ\text{C}$) in TC wakes sometimes observed in satellite images (and reproduced in our model) are spectacular but generally not relevant to the TC-ocean coupling problem.

Arguably, the mechanisms of TC intensification revealed in this regional study are essentially generic. They are very consistent with idealized cloud-resolving model studies. The presence and characteristics of mixed layers, barrier layers and oceanic eddies may vary in other cyclogenesis basins but not to the point of radically changing our results.

Finally, we have neglected the role of surface gravity waves. In case studies, age wave factors have shown to apply sensitivity to storm intensity of order 5 hPa in strong events (Doyle 2002), which is in the lower range of the SST feedback effect. The representation of the bulk effect of sea spray is also of particular interest (Bao et al. 2000) but will require higher model resolution for producing extreme wind conditions.

Acknowledgments The simulations of this study were conducted with HPC resources from the Computing Center of Region Midi-Pyrénées (CALMIP, Toulouse, France; Grants 2011, 2012, 2013—Project 1044). We also thank Alexis Chaigneau for his help on the ocean eddy tracking procedure; Florian Lemarié for his coupling algorithm and helpful discussions; and two anonymous reviewers for constructive comments.

References

- Adler R, Huffman G, Bolvin D, Curtis S, Nelkin E (2000) Tropical rainfall distributions determined using TRMM combined with other satellite and rain gauge information. *J Appl Meteorol* 39(12):2007–2023
- Balaguru K, Chang P, Saravanan R, Leung LR, Xu Z, Li M, Hsieh JS (2012) Ocean barrier layers' effect on tropical cyclone intensification. *Proc Natl Acad Sci* 109(36):14343–14347. doi:10.1073/pnas.1201364109. <http://www.pnas.org/content/109/36/14343.full.pdf+html>
- Bao JW, Wilczak JM, Choi JK, Kantha LH (2000) Numerical simulations of air-sea interaction under high wind conditions using a coupled model: a study of hurricane development. *Mon Weather Rev* 128(7):2190–2210
- Barnier B, Madec G, Penduff T, Molines JM, Treguier AM, Le Sommer J, Beckmann A, Biastoch A, Boning C, Dengg J, Derval C, Durand E, Gulev S, Remy E, Talandier C, Theetten S, Maltrud M, Mclean J, Cuevas B (2006) Impact of partial steps and momentum advection schemes in a global ocean circulation model at eddy-permitting resolution. *Ocean Dyn* 56(5–6):543–567. doi:10.1007/s10236-006-0082-1
- Bender MA, Ginis I (2000) Real-case simulations of hurricane-ocean interaction using a high-resolution coupled model: Effects on hurricane intensity. *Monthly Weather Review* 128(4):917–946. doi:10.1175/1520-0493(2000)128<0917:rcsoho>2.0.co;2
- Bender MA, Ginis I, Kurihara Y (1993) Numerical simulations of tropical cyclone-ocean interaction with a high-resolution coupled model. *J Geophys Res Atmos* 98(D12):23,245–23,263
- Brown JR, Moise AF, Colman RA (2013) The south pacific convergence zone in CMIP5 simulations of historical and future climate. *Clim Dyn* 41(7–8):2179–2197. doi:10.1007/s00382-012-1591-x
- Chaigneau A, Gizolme A, Grados C (2008) Mesoscale eddies off peru in altimeter records: identification algorithms and eddy spatio-temporal patterns. *Prog Oceanogr* 79(2–4):106–119. doi:10.1016/j.pocean.2008.10.013
- Chaigneau A, Eldin G, Dewitte B (2009) Eddy activity in the four major upwelling systems from satellite altimetry (1992–2007). *Prog Oceanogr*. doi:10.1016/j.pocean.2009.07.012
- Chang SW, Anthes RA (1978) Numerical simulations of oceans non-linear, baroclinic response to translating hurricanes. *J Phys Oceanogr* 8(3):468–480. doi:10.1175/1520-0485(1978)008<0468:nsoton.>2.0.co;2
- Charney JG, Eliassen A (1964) On the growth of the hurricane depression. *J Atmos Sci* 21:68–75
- Charnock H (1955) Wind stress on a water surface. *Q J R Meteorol Soc* 81(350):639–640. doi:10.1002/qj.49708135027
- Chauvin F, Royer JF, Deque D (2006) Response of hurricane-type vortices to global warming as simulated by ARPEGE-Climat at high resolution. *Clim Dyn* 27:377–399
- Couvelard X, Marchesiello P, Gourdeau L, Lefèvre J (2008) Barotropic zonal jets induced by islands in the southwest pacific. *J Phys Oceanogr* 38(10):2185–2204. doi:10.1175/2008JPO3903.1
- Craig G, Gray S (1996) Cisk or wishe as the mechanism for tropical cyclone intensification. *J Atmos Sci* 53(23):3528–3540. doi:10.1175/1520-0469(1996)053<3528:cowatm>2.0.co;2
- da Silva A, Young AC, Levitus S (1994) Atlas of surface marine data 1994, volume 1: algorithms and procedures. Technical report 6, U.S. Department of Commerce, NOAA, NESDIS
- de Boyer Montegut C, Madec G, Fischer AS, Lazar A, Iudicone D (2004) Mixed layer depth over the global ocean: an examination of profile data and a profile-based climatology. *J Geophys Res* 109:C12003. doi:10.1029/2004JC002378
- Debreu L, Marchesiello P, Penven P, Cambon G (2012) Two-way nesting in split-explicit ocean models: algorithms, implementation and validation. *Ocean Model*. doi:10.1016/j.ocemod.2012.03.003
- Demaria M, Kaplan J (1994) Sea-surface temperature and the maximum intensity of atlantic tropical cyclones. *J Clim* 7(9):1324–1334. doi:10.1175/1520-0442(1994)007<1324:ssstat>2.0.co;2
- Diamond HJ, Lorrey AM, Knapp KR, Levinson DH (2012) Development of an enhanced tropical cyclone tracks database for the southwest pacific from 1840 to 2010. *Int J Climatol* 32(14):2240–2250. doi:10.1002/joc.2412
- Donelan M (2004) On the limiting aerodynamic roughness of the ocean in very strong winds. *Geophys Res Lett* 31(18). doi:10.1029/2004gl019460
- Doyle J (2002) Coupled atmosphere-ocean wave simulations under high wind conditions. *Mon Weather Rev* 130(12):3087–3099. doi:10.1175/1520-0493(2002)130<3087:caowsu>2.0.co;2
- Emanuel KA (1986) An air sea interaction theory for tropical cyclones. Part I: Steady-state maintenance. *J Atmos Sci* 43(6):585–604. doi:10.1175/1520-0469(1986)043<0585:aaasif>2.0.co;2
- Emanuel KA (1988) The maximum intensity of hurricanes. *Journal of the Atmospheric Sciences* 45(7):1143–1155. doi:10.1175/1520-0469(1988)045<1143:TMIOH>2.0.CO;2
- Gentry MS, Lackmann GM (2010) Sensitivity of simulated tropical cyclone structure and intensity to horizontal resolution. *Mon Weather Rev* 138(3):688–704. doi:10.1175/2009MWR2976.1
- Gray WM (1975) Tropical cyclone genesis. Technical report no 234, Colorado State University, Fort Collins CO
- Hill K, Lackmann G (2009) Analysis of idealized tropical cyclone simulations using the weather research and forecasting model: sensitivity to turbulence parameterization and grid spacing. *Mon Weather Rev* 137(2):745–765
- Holland GJ (1997) The maximum potential intensity of tropical cyclones. *J Atmos Sci* 54(21):2519–2541. doi:10.1175/1520-0469(1997)054<2519:tmpiot>2.0.co;2
- Janjić Z (1994) The step-mountain eta coordinate model: further developments of the convection, viscous sublayer, and turbulence closure schemes. *Mon Weather Rev* 122(5):927–945
- Janssen P (1989) Wave-induced stress and the drag of air flow over sea waves. *J Phys Oceanogr* 19(6):745–754. doi:10.1175/1520-0485(1989)019<0745:wisatd>2.0.co;2
- Jourdain NC, Marchesiello P, Menkes CE, Lefevre J, Vincent EM, Lengaigne M, Chauvin F (2011) Mesoscale simulation of tropical cyclones in the south pacific: climatology and interannual variability. *J Clim* 24(1):3–25. doi:10.1175/2010jcli3559.1
- Jullien S, Menkes CE, Marchesiello P, Jourdain NC, Lengaigne M, Koch-Larrouy A, Lefevre J, Vincent EM, Faure V (2012) Impact of tropical cyclones on the heat budget of the South Pacific Ocean. *J Phys Oceanogr* 42(11):1882–1906. doi:10.1175/jpo-d-11-0133.1

- Kanamitsu M, Ebisuzaki W, Woollen J, Yang SK, Hnilo J, Fiorino M, Potter G (2002) NCEP–DOE AMIP-II reanalysis (R-2). *Bull Am Meteor Soc* 83(11):1631–1643. doi:[10.1175/bams-83-11-1631](https://doi.org/10.1175/bams-83-11-1631)
- Large W (2006) Surface fluxes for practitioners of global ocean data assimilation. In: Chassignet E, Verron J (eds) *Ocean weather forecasting*. Springer, Netherlands, Chap 9, pp 229–270. doi:[10.1007/1-4020-4028-8_9](https://doi.org/10.1007/1-4020-4028-8_9)
- Large W, McWilliams J, Doney S (1994) Oceanic vertical mixing: a review and a model with a nonlocal boundary layer parameterization. *Rev Geophys* 32(4):null-403. doi:[10.1029/94rg01872](https://doi.org/10.1029/94rg01872)
- Lemarié F (2008) Algorithmes de schwarz et couplage océan-atmosphère. PhD thesis, Université Joseph-Fourier—Grenoble I
- Lemarié F, Debreu L, Shchepetkin A, McWilliams J (2012) On the stability and accuracy of the harmonic and biharmonic isoneutral mixing operators in ocean models. *Ocean Model* 52–53:9–35. doi:[10.1016/j.ocemod.2012.04.007](https://doi.org/10.1016/j.ocemod.2012.04.007)
- Marchesiello P, McWilliams JC, Shchepetkin A (2001) Open boundary conditions for long-term integration of regional oceanic models. *Ocean Model* 3(1–2):1–20. doi:[10.1016/S1463-5003\(00\)00013-5](https://doi.org/10.1016/S1463-5003(00)00013-5)
- Marchesiello P, Debreu L, Couvelard X (2009) Spurious diapycnal mixing in terrain-following coordinate models: the problem and a solution. *Ocean Model*. 26(3–4):156–169. doi:[10.1016/j.ocemod.2008.09.004](https://doi.org/10.1016/j.ocemod.2008.09.004)
- Marchesiello P, Lefèvre J, Vega A, Couvelard X, Menkes C (2010) Coastal upwelling, circulation and heat balance around new caledonia’s barrier reef. *Mar Pollut Bull* 61(7–12):432–448. doi:[10.1016/j.marpolbul.2010.06.043](https://doi.org/10.1016/j.marpolbul.2010.06.043)
- Marchesiello P, Capet X, Menkes C, Kennan SC (2011) Submeso-scale dynamics in tropical instability waves. *Ocean Model* 39:31–46
- Menkes CE, Lengaigne M, Marchesiello P, Jourdain NC, Vincent EM, Lefevre J, Chauvin F, Royer JF (2012) Comparison of tropical cyclogenesis indices on seasonal to interannual time-scales. *Clim Dyn* 38(1–2):301–321. doi:[10.1007/s00382-011-1126-x](https://doi.org/10.1007/s00382-011-1126-x)
- Montgomery M, Sang N, RK S, Persing J (2009) Do tropical cyclones intensify by wishe. *Q J R Meteorol Soc* 135:1697–1714
- Neetu S, Lengaigne M, Vincent EM, Vialard J, Madec G, Samson G, Kumar MRR, Durand F (2012) Influence of upper-ocean stratification on tropical cyclone-induced surface cooling in the bay of bengal. *J Geophys Res Oceans* 117. doi:[10.1029/2012jc008433](https://doi.org/10.1029/2012jc008433)
- Nolan DS, Stern DP, Zhang JA (2003) Evaluation of planetary boundary layer parameterizations in tropical cyclones by comparison of in situ observations and high-resolution simulations of hurricane isabel (2003). Part II: inner-core boundary layer and eyewall structure. *Mon Weather Rev* 137(11):3675–3698. doi:[10.1175/2009MWR2786.1](https://doi.org/10.1175/2009MWR2786.1)
- Ooyama K (1969) Numerical simulation of the life cycle of tropical cyclones. *J Atmos Sci* 26:3–40
- Penven P, Debreu L, Marchesiello P, McWilliams JC (2006) Evaluation and application of the roms 1-way embedding procedure to the central california upwelling system. *Ocean Model* 12(1–2):157–187. doi:[10.1016/j.ocemod.2005.05.002](https://doi.org/10.1016/j.ocemod.2005.05.002)
- Penven P, Marchesiello P, Debreu L, Lefèvre J (2008) Software tools for pre- and post-processing of oceanic regional simulations. *Environ Model Softw* 23(5):660–662. doi:[10.1016/j.envsoft.2007.07.004](https://doi.org/10.1016/j.envsoft.2007.07.004)
- Powell M, Vickery P, Reinhold T (2003) Reduced drag coefficient for high wind speeds in tropical cyclones. *Nature* 422(6929):279–283. doi:[10.1038/nature01481](https://doi.org/10.1038/nature01481)
- Price JF (1981) Upper ocean response to a hurricane. *J Phys Oceanogr* 11(2):153–175
- Qiu B, Scott RB, Chen S (2008) Length scales of eddy generation and nonlinear evolution of the seasonally modulated south pacific subtropical countercurrent. *J Phys Oceanogr* 38(7):1515–1528. doi:[10.1175/2007JPO3856.1](https://doi.org/10.1175/2007JPO3856.1)
- Rotunno R, Emanuel KA (1987) An air-sea interaction theory for tropical cyclones. 2. Evolutionary study using a nonhydrostatic axisymmetrical numerical-model. *J Atmos Sci* 44(3):542–561. doi:[10.1175/1520-0469\(1987\)044<0542:aaitft>2.0.co;2](https://doi.org/10.1175/1520-0469(1987)044<0542:aaitft>2.0.co;2)
- Royer JF, Chauvin F, Timbal B, Araspin P, Grimal D (1998) A GCM study of the impact of greenhouse gas increase on the frequency of occurrence of tropical cyclones. *Clim Change* 38(3):307–343
- Sandery PA, Brassington GB, Craig A, Pugh T (2010) Impacts of ocean-atmosphere coupling on tropical cyclone intensity change and ocean prediction in the australian region. *Mon Weather Rev* 138(6):2074–2091. doi:[10.1175/2010mwr3101.1](https://doi.org/10.1175/2010mwr3101.1)
- Schade LR (2000) Tropical cyclone intensity and sea surface temperature. *J Atmos Sci* 57(18):3122–3130. doi:[10.1175/1520-0469\(2000\)057<3122:tciaot>2.0.co;2](https://doi.org/10.1175/1520-0469(2000)057<3122:tciaot>2.0.co;2)
- Schade LR, Emanuel KA (1999) The ocean’s effect on the intensity of tropical cyclones: results from a simple coupled atmosphere-ocean model. *J Atmos Sci* 56(4):642–651. doi:[10.1175/1520-0469\(1999\)056<0642:toseot>2.0.co;2](https://doi.org/10.1175/1520-0469(1999)056<0642:toseot>2.0.co;2)
- Schubert WH, Montgomery MT, Taft RK, Guinn TA, Fulton SR, Kossin JP, Edwards JP (1999) Polygonal eyewalls, asymmetric eye contraction, and potential vorticity mixing in hurricanes. *J Atmos Sci* 56(9):1197–1223. doi:[10.1175/1520-0469\(1999\)056<1197:PEAECA>2.0.CO;2](https://doi.org/10.1175/1520-0469(1999)056<1197:PEAECA>2.0.CO;2)
- Scoccimarro E, Gualdi S, Bellucci A, Sanna A, Fogli PG, Manzini E, Vichi M, Oddo P, Navarra A (2011) Effects of tropical cyclones on ocean heat transport in a high-resolution coupled general circulation model. *J Clim* 24(16):4368–4384. doi:[10.1175/2011jcli4104.1](https://doi.org/10.1175/2011jcli4104.1)
- Shay LK, Elsberry RL, Black PG (1989) Vertical structure of the ocean current response to a hurricane. *J Phys Oceanogr* 19(5):649–669. doi:[10.1175/1520-0485\(1989\)019<0649:vsotoc>2.0.co;2](https://doi.org/10.1175/1520-0485(1989)019<0649:vsotoc>2.0.co;2)
- Shchepetkin AF, McWilliams JC (2005) The regional oceanic modeling system (roms): a split-explicit, free-surface, topography-following-coordinate oceanic model. *Ocean Model* 9(4):347–404. doi:[10.1016/j.ocemod.2004.08.002](https://doi.org/10.1016/j.ocemod.2004.08.002)
- Skamarock WC (2004) Evaluating mesoscale NWP models using kinetic energy spectra. *Mon Weather Rev* 132(12):3019–3032. doi:[10.1175/MWR2830.1](https://doi.org/10.1175/MWR2830.1)
- Skamarock WC, Klemp JB (2008) A time-split nonhydrostatic atmospheric model for weather research and forecasting applications. *J Comput Phys* 227(7):3465–3485. doi:[10.1016/j.jcp.2007.01.037](https://doi.org/10.1016/j.jcp.2007.01.037)
- Slutz RJ, Lubker SJ, Hiscox JD, Woodruff S, Jenne R, Joseph D, Steurer P, Elms J (1985) Comprehensive ocean-atmosphere data set: Release 1. I: Climate Research Program, ERL/NOAA, Boulder CO
- Smith RK, Montgomery MT (2010) Hurricane boundary-layer theory. *Q J R Meteorol Soc* 136:1–6
- Smith RK, Montgomery MT, Nguyen SV (2009) Tropical cyclone spin-up revisited. *Q J R Meteorol Soc* 135:1321–1335
- Stern DP, Nolan DS (2011) On the height of the warm core in tropical cyclones. *J Atmos Sci* 69(5):1657–1680. doi:[10.1175/JAS-D-11-010.1](https://doi.org/10.1175/JAS-D-11-010.1)
- Sutyryn GG, Khain AP (1984) On the effect of air-ocean interaction on intensity of moving tropical cyclone. *Izvestiya, Atm Oce Phys* 20:787–794
- Vincent EM, Lengaigne M, Menkes CE, Jourdain NC, Marchesiello P, Madec G (2011) Interannual variability of the south pacific convergence zone and implications for tropical cyclone genesis. *Clim Dyn* 36(9–10):1881–1896. doi:[10.1007/s00382-009-0716-3](https://doi.org/10.1007/s00382-009-0716-3)
- Vincent EM, Lengaigne M, Madec G, Vialard J, Samson G, Jourdain NC, Menkes CE, Jullien S (2012a) Processes setting the characteristics of sea surface cooling induced by tropical cyclones. *J Geophys Res* 117:C02020. doi:[10.1029/2011JC007396](https://doi.org/10.1029/2011JC007396)

- Vincent EM, Lengaigne M, Vialard J, Madec G, Jourdain NC, Masson S (2012b) Assessing the oceanic control on the amplitude of sea surface cooling induced by tropical cyclones. *J Geophys Res* 117:C05023. doi:[10.1029/2011jc007705](https://doi.org/10.1029/2011jc007705)
- Wada A (2009) Idealized numerical experiments associated with the intensity and rapid intensification of stationary tropical-cyclone-like vortex and its relation to initial sea-surface temperature and vortex-induced sea-surface cooling. *J Geophys Res Atmos* 114(D18). doi:[10.1029/2009JD011993](https://doi.org/10.1029/2009JD011993)
- Walsh KJE, Nguyen KC, McGregor JL (2004) Fine-resolution regional climate model simulations of the impact of climate change on tropical cyclones near Australia. *Clim Dyn* 22:47–56
- Walsh KJE, Fiorino M, Landsea C, McInnes K (2007) Objectively determined resolution-dependent threshold criteria for the detection of tropical cyclones in climate models and reanalyses. *J Clim* 20(10):2307–2314
- Wang Y, Wu CC (2004) Current understanding of tropical cyclone structure and intensity changes—a review. *Meteorol Atmos Phys* 87(4):257–278. doi:[10.1007/s00703-003-0055-6](https://doi.org/10.1007/s00703-003-0055-6)
- Wu CC, Lee CY, Lin II (2007) The effect of the ocean eddy on tropical cyclone intensity. *J Atmos Sci* 64(10):3562–3578. doi:[10.1175/JAS4051.1](https://doi.org/10.1175/JAS4051.1)
- Yang B, Wang Y, Wang B (2007) The effect of internally generated inner-core asymmetries on tropical cyclone potential intensity. *J Atmos Sci* 64(4):1165–1188. doi:[10.1175/JAS3971.1](https://doi.org/10.1175/JAS3971.1)
- Zeng X, Beljaars A (2005) A prognostic scheme of sea surface skin temperature for modeling and data assimilation. *Geophys Res Lett* 32(14). doi:[10.1029/2005GL023030](https://doi.org/10.1029/2005GL023030)
- Zheng Z-W, Ho C-R, Zheng Q, Lo Y-T, Kuo N-J, Gopalakrishnan G (2010) Effects of preexisting cyclonic eddies on upper ocean responses to category 5 typhoons in the western north pacific. *J Geophys Res* 115:C09013. doi:[10.1029/2009JC005562](https://doi.org/10.1029/2009JC005562)